Biogeosciences, 21, 4637–4663, 2024
https://doi.org/10.5194/bg-21-4637-2024

Biogeosciences Open Access EGU

Temperature-enhanced effects of iron on Southern Ocean phytoplankton

Charlotte Eich[1,2,★], Mathijs van Manen[3,★], J. Scott P. McCain[4,a], Loay J. Jabre[4,b], Willem H. van de Poll[5], Jinyoung Jung[6], Sven B. E. H. Pont[1], Hung-An Tian[3], Indah Ardiningsih[3], Gert-Jan Reichart[3,7], Erin M. Bertrand[4], Corina P. D. Brussaard[1,2], and Rob Middag[3,8]

[1]Department of Marine Microbiology and Biogeochemistry, Royal Netherlands Institute for Sea Research (NIOZ), 1797 SZ 't Horntje, the Netherlands
[2]Institute for Biodiversity and Ecosystem Dynamics (IBED), University of Amsterdam, 1098 XH Amsterdam, the Netherlands
[3]Department of Ocean Systems, Royal Netherlands Institute for Sea Research (NIOZ), 1797 SZ 't Horntje, the Netherlands
[4]Department of Biology, Dalhousie University, Halifax, Nova Scotia, Canada
[5]CIO Oceans, Energy and Sustainability Research Institute Groningen, Faculty of Science and Engineering, University of Groningen, Nijenborgh 7, 9747 AG Groningen, the Netherlands
[6]Korea Polar Research Institute, 26, Songdomirae-ro, Yeonsu-gu, Incheon 21990, Republic of Korea
[7]Department of Earth Sciences, Faculty of Geosciences, Utrecht University, 3584 CB Utrecht, the Netherlands
[8]Centre for Isotope Research, CIO Oceans, Energy and Sustainability Research Institute Groningen, Faculty of Science and Engineering, University of Groningen, 9712 CP Groningen, the Netherlands
[a]current address: Department of Biology and Department of Earth, Atmospheric, and Planetary Sciences, Massachusetts Institute of Technology, Cambridge, MA 02142, USA
[b]current address: Marine Chemistry and Geochemistry Department, Woods Hole Oceanographic Institution, Woods Hole, MA 02543, USA
★These authors contributed equally to this work.

Correspondence: Charlotte Eich (charlotte.eich@nioz.nl) and Corina P. D. Brussaard (corina.brussaard@nioz.nl)

Received: 21 May 2024 – Discussion started: 24 May 2024
Revised: 3 September 2024 – Accepted: 4 September 2024 – Published: 28 October 2024

Abstract. Iron (Fe) is a key limiting nutrient for Southern Ocean phytoplankton. Input of Fe into the Southern Ocean is projected to change due to global warming, yet the combined effects of a concurrent increase in temperature with dissolved Fe (dFe) addition on phytoplankton growth and community composition have not been extensively studied. To improve our understanding of how Antarctic phytoplankton communities respond to Fe and enhanced temperature, we performed four full factorial onboard bioassays under trace-metal-clean conditions with phytoplankton communities from different regions of the Weddell Sea and the Amundsen Sea in the Southern Ocean. Treatments consisted of 2 nM Fe addition with 2 °C warming (TF), Fe addition at in situ temperature (F) +2 °C warming with no Fe addition (T) and a control at in situ temperature with no Fe addition (control, C). Temperature had a limited effect by itself but boosted the positive response of the phytoplankton to Fe addition. Photosynthetic efficiency, phytoplankton abundances and chlorophyll *a* concentrations typically increased (significantly) with Fe addition (F and/or TF treatment), and the phytoplankton community generally shifted from haptophytes to diatoms upon Fe addition. The $< 20\,\mu m$ phytoplankton fraction displayed population-specific growth responses, resulting in a pronounced shift in community composition and size distribution (mainly towards larger-sized phytoplankton) for the F and TF treatments. Such a distinct enhanced impact of dFe supply with warming on Antarctic phytoplankton size, growth and composition will likely affect trophic transfer efficiency and ecosystem structure, with potential significance for the biological carbon pump.

Published by Copernicus Publications on behalf of the European Geosciences Union.

1 Introduction

The Southern Ocean plays an important role in regulating the Earth's climate as it is an important sink for CO_2 (Takahashi et al., 2012; Friedlingstein et al., 2022; Fisher et al., 2023). Phytoplankton take up CO_2 and convert it to biomass, not only forming the base of the pelagic food web but also driving the biological carbon pump (Buesseler et al., 2020; Huang et al., 2023). During the short productive austral season, however, Antarctic phytoplankton growth often becomes limited by low iron (Fe) availability (e.g. Martin et al., 1990; Boyd, 2002; Ryan-Keogh et al., 2023). Fe is a vital micronutrient for a variety of cellular processes, including photosynthesis (Geider and La Roche, 1994; Schoffman et al., 2016; Kroh and Pilon, 2020) and nitrate assimilation (Schoffman et al., 2016; Milligan and Harrison, 2000). The shortage of Fe is a large contributing factor to the so-called high nutrient–low-chlorophyll (HNLC) conditions, where the ratio of macronutrients, especially nitrate, relative to total chlorophyll *a* (Chl *a*) concentrations is comparably high (Minas and Minas, 1992; Sarmiento et al., 2004; Venables and Moore, 2010; Basterretxea et al., 2023).

Trace metal supply in the Southern Ocean follows a strong seasonal cycle, where in winter Fe is replenished via deep water mixing (Tagliabue et al., 2014) or sediment resuspension in coastal areas (Boyd et al., 2012) and is quickly depleted again by phytoplankton uptake in the next season. Predicted increases in stratification may weaken Fe supply to surface waters from below (Sallée et al., 2021); however, this is still uncertain as increased stratification might not have a strong effect or might even increase turbulent nutrient fluxes associated with breaking internal waves (van Haren et al., 2021). Additionally, increased stratification effects may be counteracted by a deepening of mixed-layer depths (Sallée et al., 2021) and changes in gyre-scale circulations (Misumi et al., 2014). In general, Fe limitation for Antarctic phytoplankton is predicted to be at least partially relieved in the future (Bazzani et al., 2023) because of enhanced Fe supply by increased wind-driven mixing (due to reduced ice-induced stratification) and sources associated with ice melt, i.e. glaciers (Annett et al., 2015; Sherrell et al., 2015; van der Merwe et al., 2019; Seyitmuhammedov et al., 2022; Moreau et al., 2023), icebergs (Raiswell et al., 2008; Shaw et al., 2011; Raiswell et al., 2016; Hopwood et al., 2019) or sea ice (Lannuzel et al., 2016; Gerringa et al., 2020). In the Amundsen Sea, increased Fe input is likely to occur due to enhanced glacial melt and runoff, particularly during the summer months when melting is most pronounced (e.g. Van Manen et al., 2022). Increases in seawater temperature may affect the availability of Fe for phytoplankton, since temperature affects the oxidation of the bioavailable Fe(II) to Fe(III) (e.g. Millero et al., 1987); however, Aflenzer et al. (2023) did not observe a lower bioavailability of added Fe with increased temperatures. In the Weddell Sea, Fe input may increase through upwelling of Fe-rich deep waters and meltwater from ice shelves, but this is less certain (Klunder et al., 2011). Seasonal variations in sea ice cover and glacial melt will play a significant role in determining the timing and magnitude of Fe input in these regions. These changes in Fe supply are associated with ongoing climate change, which is projected to lead to elevated temperatures and changes in wind patterns as well as associated currents and upwelling (Turner et al., 2005; Moore et al., 2018). Overall, future Southern Ocean conditions will most likely be warmer with potentially elevated Fe concentrations, which can be expected to also affect phytoplankton productivity and community composition (Boyd et al., 2015; Laufkötter et al., 2015; Pinkerton et al., 2021). Depending on the geographical region and the time in the productive season (Thomalla et al., 2023), global warming is predicted to increase wind-induced mixing or strengthen vertical stratification (Bronselaer et al., 2020; De Lavergne et al., 2014; Hillenbrand and Cortese, 2006; Shi et al., 2020). Phytoplankton will bloom earlier in the productive season as a result of decreasing sea ice and consequently higher light (Krumhardt et al., 2022), most likely rapidly drawing down available Fe followed by stratification and thus creating favourable conditions for smaller-sized phytoplankton (Deppeler and Davidson, 2017; Krumhardt et al., 2022). Besides Fe and temperature, there are also other factors, e.g. other bio-essential metals (Mn, Co, Ni, Cu and Zn), where notably Mn has been shown to be (co-)limiting in the Southern Ocean (Wu et al., 2019; Browning et al., 2021; Balaguer et al., 2022; Hawco et al., 2022). Mn is essential for phytoplankton photosystems (Raven et al., 1990) and is a co-factor for enzymes dealing with oxidative stress (Wolfe-Simon et al., 2005). Moreover, light is another major limiting factor for phytoplankton growth in the Southern Ocean (e.g. van Oijen et al., 2004; Strzepek et al., 2019; Vives et al., 2022; Latour et al., 2024).

Considering the urgency of warming and the anticipated change in Fe supply, there is a need for studies that investigate the combined effects of these two important drivers controlling phytoplankton growth in the Southern Ocean. There are many reports on the effects of Fe addition to Fe-limited phytoplankton from the Southern Ocean (reviewed by, for example, Yoon et al., 2018, and Bazzani et al., 2023) and several on the influence of temperature (Reay et al., 2001; Morán et al., 2006; Boyd et al., 2013), but only a few studies have examined the combined effects of Fe and temperature on Antarctic phytoplankton (i.e. Rose et al., 2009; Zhu et al., 2016; Andrew et al., 2019; Jabre and Bertrand, 2020; Jabre et al., 2021; Aflenzer et al., 2023). In particular, studies using natural phytoplankton communities are scarce (Rose et al., 2009; Jabre et al., 2021) and are concentrated on Ross Sea phytoplankton with relatively large temperature increases (3 to 6 °C). Hence, more insight into how phytoplankton from other regional Antarctic seas respond to the warming projected by the year $\sim$ 2100 (Meredith et al., 2019) is needed.

The Weddell Sea is one of the key areas of dense Antarctic bottom-water formation (Fahrbach et al., 2004) and plays

an important role in the global thermohaline circulation. The subpolar cyclonic Weddell Gyre circulating in the Weddell Sea basin isolates the centre of the Weddell Sea from marginal Fe sources such as melt or sediments, whilst the currents on the edges of the gyre have the potential to pick up Fe from a variety of sources, such as the seafloor, bathymetry-driven mixing with deeper water masses, and sources associated with ice melt (Klunder et al., 2014; Sieber et al., 2021; Tian, 2024). Generally, the Weddell Sea has relatively low primary productivity, associated with Fe limitation in the centre of the gyre (Hoppema et al., 2007; Klunder et al., 2014). In contrast, the western Amundsen Sea, specifically the Amundsen Sea Polynya (ASP), is known as one of the most productive regions in the Southern Ocean in terms of net primary production per net area (Arrigo and van Dijken, 2003). Additionally, this region (ASP) is characterized by a fast thinning of ice sheets, shelf ice and glaciers, with associated input of Fe required to sustain the high levels of primary productivity (e.g. Gerringa et al., 2012; van Manen et al., 2022). Nevertheless, phytoplankton in the ASP could still be stimulated by additional Fe input (Alderkamp et al., 2015).

The aim of the current study is to examine the concurrent effects of Fe supply and warming on Antarctic phytoplankton communities from the Weddell Sea and the Amundsen Sea under controlled trace-metal-clean conditions. Given the naturally low dissolved Fe (dFe) concentrations in the Southern Ocean, trace-metal-clean conditions are crucial to avoid confounding Fe effects when studying temperature alone (Middag et al., 2023). Our bioassay treatments comprised a full factorial combination of dFe and temperature increases. The temperature was enhanced by 2 °C, based on forecasts from an IPCC report (Meredith et al., 2019). Whilst the Amundsen Sea has already shown a warming trend over the past years (Gómez-Valdivia et al., 2023; Drijfhout et al., 2024), the surface waters of the Weddell Sea have not (yet) shown a clear increasing temperature trend, but underlying waters are warming (Strass et al., 2020), and local temperature increases due to upwelling of warm deep water have been observed (Darelius et al., 2023; Teske et al., 2024). The concentration of dFe in the Fe-addition treatments (F and TF) was increased by 2 nM. Future Fe concentrations are highly uncertain (Hutchins and Boyd, 2016; Tagliabue et al., 2016; Ryan-Keogh et al., 2023) and not necessarily linked to the bioavailability of Fe (Van Manen et al., 2022; Fourquez et al., 2023), but previous experiments in the Southern Ocean have shown that such an addition represents (temporarily) Fe-replete conditions (De Baar et al., 2005). Moreover, increased Fe availability in the Southern Ocean could have a far-reaching impact, leading to increased nutrient consumption and consequently reducing nutrient transfer to lower latitudes where primary production is fuelled by these nutrients (Primeau et al., 2013; Moore et al., 2018). By integrating biological and trace metal chemistry analyses within large-volume (20 L Cubitainers), trace-metal-clean experiments, we aim to provide a clearer understanding of future changes in phytoplankton growth patterns and the implications for the Southern Ocean's role in global climate regulation.

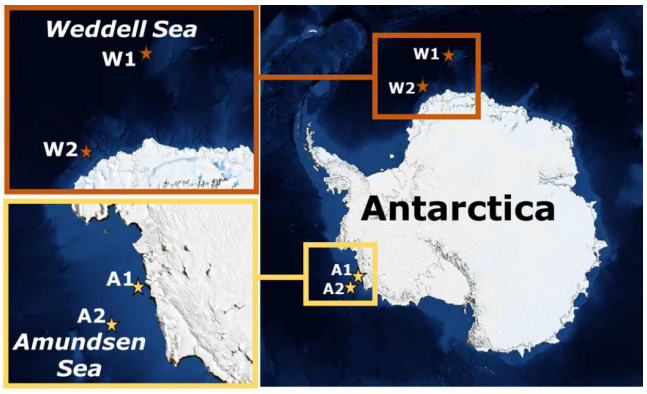

Figure 1. Location of the four bioassay experiments: bioassays A1 and A2 were performed in the Amundsen Sea and W1 and W2 in the Weddell Sea (image obtained from NASA Worldview).

2 Material and methods

2.1 Location and sampling

Natural seawater for the bioassays was collected during research expeditions (Fig. 1) in the Amundsen Sea (bioassays A1 and A2, R/V *Araon*, ANA08B, 2017/18) and in the Weddell Sea (bioassays W1 and W2, R/V *Polarstern* (Alfred-Wegener-Institut Helmholtz-Zentrum für Polar- und Meeresforschung, 2017), PS117, 2018/19) in austral summer (December–February).

Seawater was sampled at the autofluorescence maximum (36 m for A2 and 20 m for both W1 and W2), except for bioassay A1, which did not show an autofluorescence maximum and was sampled at the mid-mixed-layer depth (15 m). Water for each bioassay was collected in a single deployment of the Royal Netherlands Institute for Sea Research (NIOZ) Titan ultraclean CTD sampling system for trace metals (De Baar et al., 2008), mounted with PRISTINE large-volume samplers (Rijkenberg et al., 2015). To prevent light shock for the phytoplankton, the original polyvinylidene fluoride (PVDF) PRISTINE samplers were replaced by a light-proof polypropylene version. Salinity (conductivity), temperature, fluorescence, depth (pressure) and oxygen were measured with a CTD instrument (Sea-Bird SBE 911plus) mounted on the trace-metal-clean sampling system (De Baar et al., 2008). To avoid contamination, further processing was performed under trace-metal-clean, dimmed-light conditions and at 2 °C in a clean-room environment inside a modified high-cube shipping container which fits the Titan sampling system. During transport on deck, Cubitainers were covered with black light-proof bags to avoid light stress.

Water for Amundsen Sea bioassay A1 was sampled from the middle of the ASP, and for bioassay A2 it was sampled in the marginal sea ice zone just outside of the ASP. Both W1 and W2 were performed with water from the eastern Weddell Sea. The Amundsen Sea bioassays A1 and A2 ran for 6 d (25 to 31 January and 31 January to 6 February 2018, respectively), whilst the Weddell Sea bioassays W1 and W2 ran for 8 d (28 December 2018 to 5 January and 9 to 17 January 2019, respectively; see Fig. S1 in the Supplement for regional Chl *a* concentrations at the start of bioassay incubations and Fig. S2 for station depth profiles). Amundsen Sea bioassays were thus initiated towards the end of the reported bloom period (Arrigo et al., 2012), whilst Weddell Sea bioassays were initiated during the start of the bloom period (von Berg et al., 2020).

2.2 Bioassay incubation set-up

Incubations were performed in custom-built deck incubators (see the Supplement, "Bioassay set-up", for more information). Collapsible 20 L Cubitainers (LDPE with PP caps and fitted with PE faucets; Cole-Parmer, IL, USA) were used. These were soap-cleaned and HCl-cleaned (1 M) prior to the expeditions and stored with full surface contact in 0.024 M HCl (VWR NORMATOM ultrapure, Avantor, Radnor, PA, USA) for at least 2 months. Before use, Cubitainers were rinsed five times with ambient seawater. The natural seawater for the actual incubations was distributed randomly to the total of 12 Cubitainers, which were then randomly assigned to the different treatments. Trace-metal-clean conditions were maintained during all sampling and sample handling.

The bioassay treatments (performed in triplicate) were in situ conditions (control, C), +2 nM dFe (as $FeCl_3$) addition (F), +2 °C temperature increase (T), and +2 nM dFe addition and +2 °C temperature increase (TF). For the Amundsen Sea bioassays, a natural isotopic composition (natural dFe) was used for the dFe addition, whilst d^{57}Fe was used in the Weddell Sea bioassays. This practice was adopted to better differentiate the added Fe from the naturally present Fe, as we noticed that the dFe concentration in Fe-amended Amundsen Sea bioassays quickly returned to background concentrations (see Sect. 3.1). Measuring Fe with a natural isotopic composition at these low concentrations is still a challenge, especially when combined with inherent variability between replicates. After several days it became impossible to distinguish the Fe-amended and non-amended treatments in Amundsen Sea bioassays based on their natural dFe concentration (see Sect. 3.1). The variation in natural dFe expected between Fe-amended and non-amended treatments despite precipitation and uptake was hidden in the analytical and environmental variability. For Weddell Sea bioassays, we thus decided to add ^{57}Fe, a rare (2.12 % abundance vs. 91.75 % for ^{56}Fe) natural isotope of Fe. Given its low natural abundance, ^{57}Fe is not nearly as sensitive to analytical and replicate variation, as such variation is insignificant relative to the addition, allowing better insight into Fe drawdown over the course of the experiments.

Average starting concentrations of dFe in the Fe-addition treatments ranged from 2.03 to 2.28 nM for both Weddell Sea and Amundsen Sea bioassays. Temperatures in the T and TF treatments were 1.4, 0.4, 1.7 and 1 °C for A1, A2, W1 and W2, respectively (see Table 1 for an overview of starting conditions in all treatments). One replicate of the control treatment in bioassay W1 started leaking during the incubation and was thus not sampled from day 4 onwards. For bioassay W2, the in situ temperature of −1.4 °C could not be maintained due to the very sunny weather, resulting in an increase of 0.4 °C for all treatments. Final incubation temperatures were −1.0 °C in the control (C) and Fe-only (F) treatment and 1 °C (instead of 0.6 °C) in the T and TF treatments. This temperature adjustment was done slowly over the course of 24 h on the second day of the incubation. More details about the set-up can be found in the Supplement data (Fig. S3 showing the bioassay set-up). Over the course of the incubation period, temperatures were kept constant, with a maximum temperature fluctuation of ± 0.3 °C.

For Amundsen Sea bioassays, light levels were chosen to mimic in situ conditions, but noting the low-light conditions during these incubations (ca. 3 % of in-air photoactive radiation, PAR, i.e. average 3.4 and 1.5 µmol quanta m^{-2} s^{-1} for A1 and A2 over the course of incubation), we opted for non-limiting light conditions (Bertrand et al., 2011) for the (later-performed) bioassays of the Weddell Sea (ca. 12 % of in-air PAR, i.e. average 69 and 100 µmol quanta m^{-2} s^{-1} for W1 and W2 over the course of incubation). The percentages and values reported refer to approximate light conditions within Cubitainers. Light levels were adapted using neutral density screens. Samples for dissolved and particulate metals, Chl *a*, pigment-based taxonomic analyses, particulate organic carbon (POC), particulate organic nitrogen (PON), and particulate organic phosphate (POP) were taken before filling of the Cubitainers at the start of the bioassay incubations (t_0) and at the end of the incubations after 6 d (Amundsen Sea) or 8 d (Weddell Sea) (difference in duration due to logistical constraints). Samples for phytoplankton photosynthetic efficiency (F_v/F_m) and phytoplankton abundances were taken at least every other day. Macronutrients were measured on board at least every other day to screen for potential macronutrient limitation.

2.3 Set-up verification

To test for potential Fe contamination, three Cubitainers were filled with ultrapure (UP) water and handled and subsampled using the same methods and frequency as the treatments. Subsamples for dFe analysis were taken at the start (0.08 ± 0.04 nM) and after 3 d (0.07 ± 0.04 nM) and 6 d (0.06 ± 0.04 nM). Concentrations of dFe stayed consistently low, suggesting minimal or no contamination. We also tested whether added dFe stayed in solution or adsorbed to the Cu-

Table 1. Characteristics of the seawater used for the bioassay experiments. Lat. denotes latitude, Long. denotes longitude, Temp. denotes temperature, Si denotes silicate, PO_4 denotes phosphate, NO_x denotes nitrate + nitrite, dFe denotes dissolved iron, Chl *a* denotes chlorophyll *a*, Phyto denotes total flow-cytometry-based phytoplankton abundances, F_v/F_m denotes the photosynthetic capacity of the total phytoplankton and r.u. denotes relative unit. The reported irradiance is the average irradiance at the sampling depth on the day of sampling.

Bioassay	Station	Lat. (° S)	Long. (° W)	Temp. (°C)	Salinity (psu)	Irradiance (µmol quanta m^2 s^{-1})	Si (µM)
A1	31	73.50	116.50	−0.6	33.99	5.0	77.9
A2	52	72.00	118.42	−1.6	33.89	3.1	77.5
W1	17	65.00	000.00	−0.3	33.90	17.7	58.3
W2	36	70.08	011.08	−1.4	33.82	97.6	71.8

Bioassay	PO_4 (µM)	NO_x (µM)	dFe (nM)	total Chl *a* (µg L^{-1})	< 20 µm Chl *a* (%)	Phyto (× 10^3 mL^{-1})	F_v/F_m (r.u.)
A1	1.8	24.3	0.28	3.0	42	8.4	0.6
A2	2.0	28.2	0.10	0.4	98	7.1	0.6
W1	1.6	24.0	0.05	1.5	24	5.6	0.3
W2	1.9	27.9	0.03	0.6	65	4.4	0.3

bitainer walls, and we found a slow gradual decrease over the first few days in dFe concentrations after addition to UP water that we attribute to precipitation and wall adsorption (Table S1). During our experiments, the concentrations of added dFe decreased more rapidly, whereas the dFe concentrations in the non-Fe treatments, as well as the non-added form of dFe in Fe treatments ($d^{57}Fe$ for Amundsen Sea and natural dFe for Weddell Sea bioassays), stayed low and relatively constant over time. Since phytoplankton grew in all treatments, the faster decrease in added dFe was likely due to uptake and sorption onto (biogenic) particles rather than precipitation to the Cubitainer walls. Low traceable amounts of $d^{57}Fe$ during the second half of the incubations in W1 and W2 suggested that the initial decrease in dFe concentrations did not correspond to permanent removal from the bioavailable Fe pool (e.g. due to absorption; Jensen et al., 2020) but instead buffered the dissolved pool (as suggested for natural settings with exchange between the (labile) particulate iron (pFe) and dFe pools; Van Manen et al., 2022) or that most of the added dFe was taken up by phytoplankton as rapid luxury uptake during the first days of an experiment (Lampe et al., 2018).

2.4 Macronutrients

During the Amundsen Sea bioassays, dissolved macronutrients were measured on board following Jeon et al. (2021) according to the Joint Global Ocean Flux Study (JGOFS) protocols (Gordon et al., 1993) using a four-channel autoanalyser (QuAAtro, Seal Analytical, Norderstedt, Germany). Measurement precision values were ± 0.02, ± 0.28 and ± 0.14 µM for phosphate, silicate and nitrogen (nitrate + nitrite), respectively (Jeon et al., 2021). For Weddell Sea bioassays, samples for nitrate, nitrite, phosphate and silicate were measured following the method described by Gerringa et al. (2019). Measurement precision values were ± 0.01, ± 0.31 and ± 0.04 µM for phosphate, silicate and nitrogen (nitrate + nitrite), respectively.

2.5 Dissolved and particulate metals

Cubitainers were subsampled for dFe as well as other dissolved trace metals (dMn, dCo, dCu, dNi, dZn, dCd) using a 0.2 µm Sartobran 300 filter cartridge (Sartorius AG, Göttingen, Germany) for bioassays A1 and A2 and pre-acid-cleaned 0.2 µm AcroPak filter cartridges (Cytiva, Marlborough, MA, USA) for W1 and W2. Filters were fitted to an UP-cleaned vented PE faucet attached to the Cubitainer with HCl-acid-cleaned (1.5 M) silicon tubing. Filtered samples were taken by applying pressure to the Cubitainer. Different filters were used for Fe-replete and Fe-deplete treatments, and filters were replaced between experiments. The dissolved trace metal samples were collected in acid-cleaned 125 mL LDPE bottles following GEOTRACES protocols (Cutter et al., 2017) and directly acidified by adding ultrapure HCl (Baseline® HCl; Seastar Chemicals Inc, Sidney, Canada), resulting in a concentration of 0.024 M with a final pH of ∼ 1.8. Samples were stored until analysis at NIOZ. Trace metal samples were prepared and analysed following van Manen et al. (2022) and references within. In short, trace metal samples were preconcentrated using a seaFAST preconcentration system (ESI). Blank contributions from sample handling, preconcentration and analysis steps were determined by analysing acidified Milli-Q (MQ) water (∼ pH 1.8) prepared in the same way as real samples.

For particulate trace metals (pFe, pMn, pCo, pCu, pZn, pCd, pAl) and POP, 25 mm polyethersulfone (PES) disc filters (0.45 µm Pall Supor, Port Washington, NY, USA) and polypropylene filter holders (Advantec, Cole-Parmer, Vernon Hills, IL, USA) were used, following the protocol adapted

by van Manen et al. (2022) with one additional step: samples were soaked for at least 30 min in oxalate–EDTA (0.75 and 5.5 M, respectively) in a 10 L carboy (VWR Collection; Avantor, Radnor, PA, USA) to remove all trace metals outside or adsorbed to phytoplankton cell walls (modified after Hassler and Schoemann, 2009) and subsequently filtered. The EDTA oxalic acid wash used on particulate samples prior to filtration should effectively remove surface-bound metals, also minimizing the authigenic Fe fraction. Due to time limitations, samples for particulate metals were only taken during experiments A1, W1 and W2. After filtration, which happened at the end of the experiments, filters were stored frozen at −20 °C until analysis. In the NIOZ lab, filters were treated with two successive digestion steps to determine the total particulate fraction. All vials used in the digestion procedures were rigorously cleaned with HF and HCl beforehand and rinsed with UP water. Filters were subjected to a leach consisting of 1.8 mL of 4.35 M (25 %) distilled acetic acid that has been sub-boiled twice and 0.02 M (2 %) hydroxylamine hydrochloride (99.999 % trace metal basis, Sigma-Aldrich, St Louis, MO, USA). Subsequently, filters were digested following the total digestion protocol developed by Cullen and Sherrell (1999) and modified by Planquette and Sherrell (2012). A volume of 2 mL of distilled 8.0 M (50 %) HNO_3 that had been sub-boiled three times (VWR Chemicals – AnalaR NORMAPUR, Avantor, Radnor, PA, USA) and 2.9 M (10 %) HF (Merck – Supelco, Kenilworth, NJ, USA) was added. The vials were closed tightly and refluxed for 4 h at 110 °C. The solution was then transferred to a secondary Teflon vial and were then heated to near dryness at 110 °C. A 1 mL volume of 8.0 M (50 %) distilled HNO_3 that had been sub-boiled three times (VWR Chemicals – AnalaR NORMAPUR, Avantor, Radnor, PA, USA) and 15 % H_2O_2 (Merck – Suprapur, Kenilworth, NJ, USA) was added to the dried vial contents. The vials were refluxed for 1 h at 110 °C and subsequently cooled to room temperature. Addition of reagents and refluxing were repeated once. After this repetition, the vials were heated to near dryness at 110 °C. The samples were re-dissolved in 2 mL 1.5 % distilled HNO_3 that has been sub-boiled three times with 10 ppb Rh as the internal standard and were transferred to 2 mL Cryovials® (VWR Chemicals, Avantor, Radnor, PA, USA) for storage and analysis.

The lithogenic fraction and concentration of pFe and other particulate metals discussed were determined by assessing the ratio between the particulate metal of interest and particulate aluminium (pAl), assuming all pAl originates from crustal material using the approach described in more detail in van Manen et al. (2022). For example, we use the observed pFe / pAl ratio in the samples and the known crustal ratio of 0.21 mol mol^{-1} (Taylor and McLennan, 1985) to calculate the lithogenic pFe fraction and concentration.

2.6 ICP-MS trace metal measurements and particulate organic phosphorous

Dissolved trace metal samples were preconcentrated using a seaFAST preconcentration system (ESI) using two loops of 10 mL and were eluted into 350 µL elution acid (1.5 M Teflon distilled HNO_3 with rhodium as the internal standard), which gives a preconcentration factor of 57.14 (see van Manen et al., 2022). Dissolved trace metal samples, blanks (Table S2) and references (Table S3) were analysed by inductively coupled plasma mass spectrometry (ICP-MS; Thermo Scientific sector field high-resolution Element 2, Thermo Fisher Scientific, Waltham, MA, USA). Blank values were much lower than the analysed samples, and reference results were in good agreement with certified values.

For the particulate samples, including POP, the procedure blanks without a filter were treated identically to the samples, except for the steps involving filter handling and the removal of the filter from the filter holders. Therefore, the vial blank is included in this reagent blank. Filter blanks consisted of unused acid-cleaned PES disc filters (Table S4).

The accuracy and precision of the digestions were assessed by certified reference materials (CRMs). There is no CRM available for marine suspended particulate matter; therefore accuracy could only be approximated by analysis of other available CRMs. PACS-2 and MESS-3 (marine sediments, National Research Council of Canada) were analysed. For each CRM, 10–30 mg was digested, whilst recommended sample weights are 250 mg for PACS-2 and MESS-3. The lower sample weights in this study were chosen to be representative of actual concentrations of marine suspended particulate matter (similarly to in Ohnemus et al., 2014). PACS-2 and MESS-3 were only subjected to the total digestion (Table S5). The CRMs were in good agreement with the certified values.

2.7 Particulate organic carbon and nitrogen

For POC and PON sampling, 1 L of unfiltered seawater was collected from each Cubitainer and stored in dark bottles (Nalgene, Rochester, NY, USA) at 1 °C until further processing (within 4 h of sampling). Filtration was then performed using combusted (4 h at 500 °C; Verardo et al., 1990) 0.3 µm 25 mm GF75 filters (Whatman, Cytiva, Maidstone, UK) under modest pressure (max 200 mbar). Filters were folded once, packed in aluminium foil and stored frozen (−20 °C) until analysis. The POC and PON concentrations were measured using a Thermo Interscience Flash EA 1112 series elemental analyser (Thermo Scientific, Waltham, MA, USA) with excess oxygen at 900 °C and with a detection limit of 100 ppm and a precision of 0.3 % (Verardo et al., 1990). Before analysis, GF75 filters were folded and packed into a tin cup. The instrument blank is included by the analyser calibration. The carbon and nitrogen contents of samples and blanks were computed according to the results of the standard mea-

surements, and the blank was subtracted from the sample. Acetanilide (C_8H_9NO) with 71.09 % C and 10.36 % N (ThermoQuest, Milan, Italy) was measured as the standard material, and silty and sandy soil standards from Elemental Microanalysis were measured as an internal reference.

2.8 Phytoplankton photosynthetic efficiency

F_v/F_m was determined in a WATER-K quartz cuvette (3.5 mL) using pulse-amplitude-modulated fluorometry (Heinz Walz WATER-PAM, with Red LED WATER-ED cuvette version S/N EDEE0196, Heinz Walz GmbH, Effeltrich, Germany). Samples were kept in 50 mL Greiner tubes (Thermo Fisher Scientific, Waltham, MA, USA) in the cold (stored in a cool box on ice) and in the dark for dark adaptation (15 min up to occasionally 4 h). Acclimation times of up to 4 h did not affect the photosynthetic efficiency of different phytoplankton (Louis Peperzak, personal communication, 2018; Eich et al., 2021). The measuring light frequency used was set to level 5 (25 Hz) with an intensity of 8, the saturation pulse width was set to 0.8 s, and the far-red pulse width was set to 10 s with intensities of 10 and 6 each. The cuvette was rinsed with ultrapure (UP) water between samples, which was removed by shaking the cuvette and placing it upside down on lint-free paper towels to remove any remaining droplets (testing technical replicates did not show a significant effect of UP rinsing; non-parametric Kruskal–Wallis ANOVA, $p = 0.95$). The relative fluorescence yield (F_t) values were kept between 100 and 1000 by adjusting the photomultiplier (PM) gain. Blanking was done for each station and/or bioassay using 0.2 µm filtered seawater (Cullen and Davis, 2003) from the respective stations and was repeated after PM-gain adjustment when needed. The following formula was used to obtain the photosynthetic efficiency: $F_v/F_m = (F_m - F_0)/F_m$, with F_0 being the minimum fluorescence and F_m being the maximum fluorescence.

2.9 Chlorophyll *a* concentration and pigment-based taxonomic analyses

Samples (0.54–2.65 L) for Chl *a* concentrations and pigment-based community composition were filtered within 30 min of subsampling (kept on ice and in the dark) on GF/F glass fibre filters (25 mm diameter, Whatman, Cytiva, Marlborough, MA, USA) using a vacuum pump (max 200 mbar) until filters showed clear colouring. Samples were taken for total Chl *a* concentration as well as a < 20 µm fraction for better compatibility with phytoplankton community measurements by flow cytometry. For the < 20 µm fraction, natural seawater was reverse-sieved through a 20 µm mesh before filtration onto a GF/F filter. Due to low sample volume availability at bioassay A2, the same amount of water from all replicates was combined for both total and < 20 µm Chl *a* samples, resulting in one averaged value for each treatment. Filters were folded once and double-wrapped in aluminium foil, flash-frozen in liquid nitrogen, and stored at −80 °C until further analysis in the home lab. Pigments were dissolved in 90 % acetone from the freeze-dried filters according to Van Leeuwe et al. (2006), and high-performance liquid chromatography (HPLC) pigment separation was performed (ZORBAX Eclipse XDB-C8 column, 3.5 µm particle size) according to Van Heukelem and Thomas (2001). Detection of pigments was based on both the retention time and diode array spectroscopy of standards (346 nm, Waters 996), and quantification was based on calibration curves using those standards (DHI LAB standards). Phytoplankton community composition was determined using CHEMTAX version 1.95 (Mackey et al., 1996), following Selz et al. (2018). For the final pigment ratios, see Table S6.

2.10 Phytoplankton and bacterial abundances (< 20 µm)

Phytoplankton cell abundances (< 20 µm) were obtained using a 488 nm argon laser benchtop Becton, Dickinson and Company FACSCalibur (BD Biosciences, Franklin Lakes, NJ, USA) flow cytometer with the trigger set on red Chl *a* autofluorescence (Marie et al., 1999). The phytoplankton samples from the Amundsen Sea bioassays were measured freshly within 30 min of sampling (stored on ice); the Weddell Sea bioassay phytoplankton samples were fixed for 15–30 min with 100 µL formaldehyde–hexamine (18 % *v*/*v* : 10 % *v*/*v*) at 4 °C, flash-frozen in liquid nitrogen and stored at −80 °C until analysis in the home lab. Phytoplankton populations were differentiated based on their red autofluorescence and side scatter, using FCS Express 5 (De Novo Software, Pasadena, CA, USA). Freshly counted samples resulted in gating comparable to that of the fixed samples (tested for Amundsen Sea samples).

A total of 25 populations were distinguished (Table S7), whereby not all populations occurred in both seas and all bioassays. Average cell diameters were determined by size fractionation, i.e. serial gravity filtration through 20, 10, 8, 5, 3, 2, 1, 0.8 and 0.6 µm PC filters (Whatman, Cytiva, USA, Marlborough, MA, USA) using a reusable filter holder (Whatman, Cytiva, Marlborough, MA, USA) and a plastic syringe. The numbers of cells retained by each filter per discriminated population were plotted against the respective filter size. The average cell diameters were defined as the size where 50 % of the original number of cells was retained, based on the fit of a sigmoidal plot (Veldhuis and Kraay, 2004). Phyto 5, Phyto 6, Phyto 7, Phyto 11, Phyto 12 and Phyto 14 (with "Phyto" and a numeral denoting phytoplankton population groups) were cryptophytes that were identified by their orange phycoerythrin autofluorescence. Based on earlier work (Biggs et al., 2019), we consider phytoplankton populations Phyto 20 and Phyto 22 to Phyto 25 to be diatoms and Phyto 8 to be *Phaeocystis antarctica* by comparing the red autofluorescence and side-scatter pattern of the respective phytoplankton groups. The latter was confirmed

during the Amundsen Sea expedition when we selectively collected *Phaeocystis* colonies and analysed them freshly on board after gentle shaking (to break up the colonies). Phytoplankton carbon was estimated based on the cell volume of phytoplankton, assuming spherical cells, and using 237 fg C μm^{-3} for picophytoplankton populations Phyto 1 to Phyto 6 and 196.5 fg C μm^{-3} for nanophytoplankton populations Phyto 7 to Phyto 25 (Garrison et al., 2000; Worden et al., 2004). Phytoplankton net growth rates were calculated using exponential trend lines. For total abundances, the full incubation period was taken into account (i.e. days 1–6 for Amundsen Sea and days 2–8 for Weddell Sea bioassays). Starting abundances were taken prior to filling of the Cubitainers and hence were not taken into account. For the phytoplankton-group-specific rates, only those time points (at least three but most often four to five time points) with a consecutive increase in abundances were selected.

Samples for bacterial abundances were fixed with EM-grade glutaraldehyde (0.5 % final concentration; Sigma-Aldrich, Zwijndrecht, the Netherlands), flash-frozen in liquid nitrogen and stored at −80 °C until analysis using flow cytometry (Marie et al., 1999). Bacterial carbon concentrations were calculated assuming 12.4 fg C per cell (Fukuda et al., 1998).

2.11 Statistical analyses

All statistical analyses were performed using R (R Core Team, 2021). Plots were made using ggplot2 (Wickham, 2016). To detect differences in phytoplankton community composition between treatments, an analysis of similarities (ANOSIM) was performed (vegan library, using Bray–Curtis dissimilarity with 9999 permutations). When a significant difference ($p < 0.05$) was detected, an indicator species analysis (vegan library, function r.g. with 9999 permutations) was used as a follow-up analysis to see which phytoplankton groups differed between treatments. This was done for both flow-cytometry-based abundances and pigment-based taxonomic group composition, using relative values, normalized against total Chl *a* for pigment-based community composition and total phytoplankton abundance for both pigment-based and flow-cytometry-based phytoplankton groups. For the indicator species analysis (indicspecies library; De Cáceres and Legendre, 2009), *p* values are reported. A Scheirer–Ray–Hare test (non-parametric ANOVA-like test, rcompanion library; Mangiafico, 2023) was performed to determine the significance of Fe addition and temperature increase, as well as potential interaction effects, on the respective response variable measured. The test was performed for data of the last day of the incubation, since effects were usually strongest then, and some variables were only sampled at the beginning and the end of the experiment (day 6 for A1 and A2, day 8 for W1 and W2). We manually calculated eta-squared (η^2, amount of variance explained; the higher the value, the larger the effect) by dividing the sum of squares of the effect of interest (i.e. iron addition, temperature increase and the interaction between these two) by the total sum of squares. η^2 is provided when temperature increase, iron addition and/or the interaction between both was found to be significant. Since we wanted to look at the overall effect of Fe addition, temperature increase and potential interaction effects on total phytoplankton abundances based on flow cytometry, we additionally applied a generalized linear model (GLM, emmeans library; Lenth, 2024), assuming a quasi-Poisson distribution in combination with a log-link function, including the bioassay as well as the day number as factors without interaction and including an interaction term for the Fe and temperature treatment. For the GLM, the data of all bioassays and all time points (excluding day 0) were combined. The formula for the GLM was total phytoplankton abundances ∼ Fe treatment × temperature treatment + bioassay + day number. Statistical results are only reported for variables where more than one replicate was available. We also performed an NMDS (non-metric multidimensional scaling, vegan library) analysis based on phytoplankton abundances using the vegan library with Bray–Curtis dissimilarity (seed set to 123). A significance level of $p < 0.05$ was used. Where applicable, the mean ± standard deviation is reported, unless stated otherwise. All statistical results are reported in the Supplement (Tables S9–S20).

3 Results

3.1 Sample site characteristics

The in situ temperature was below 0 °C for all bioassays, with the lowest values for Amundsen Sea bioassay A2 and Weddell Sea bioassay W2 (−1.6 and −1.4 °C, respectively, compared to −0.6 and −0.3 °C for A1 and W1, respectively). The daily average irradiance at sampling depth on the day of sampling was lowest for A1 and A2, i.e. < 6 µmol quanta m^{-2} s^{-1}, compared to 18 and 98 µmol quanta m^{-2} s^{-1} for W1 and W2. Dissolved inorganic macronutrient concentrations were relatively comparable between bioassays, except the silicate concentration in W1 being ∼ 20 µM lower than for the other bioassays (but still far from limiting). Initial dFe concentrations in the Weddell Sea were lower compared to the Amundsen Sea (Table 1), as were dMn concentrations (Fig. 2). Bioassay A1 had the highest Chl *a* concentrations (sampled within the ASP), followed by W1. Both bioassays also had the highest share of > 20 µm Chl *a*. The Chl *a* concentration of A2 was almost exclusively made up of < 20 µm sized phytoplankton (98 % of total Chl *a*, Table 1). Flow-cytometry-derived phytoplankton abundances were highest for the Amundsen bioassays. The photosynthetic efficiency F_v/F_m at the start of the incubations was 2-fold lower for the Weddell Sea bioassays compared to the Amundsen Sea bioassays (i.e. 0.3 vs. 0.6 r.u., respectively). The station for bioassay W2 was closest to the

coast, followed by A1, A2 and W1; however distance to land did not seem to have a major impact on either phytoplankton community composition or nutrient concentrations.

3.2 Nutrient dynamics

Bioassay treatments without Fe addition (C and T) started at naturally low dFe concentrations (0.28 ± 0.16, 0.10 ± 0.02, 0.05 ± 0.03 and 0.03 ± 0.01 nM natural dFe for bioassays A1, A2, W1 and W2, respectively) and stayed within these ranges. The Fe-addition treatments (F and TF) showed a rapid (and overall comparable) drawdown of the added Fe (natural Fe for A1 and A2 – Fig. 2a, b; $d^{57}Fe$ for W1 and W2 – Fig. 2e, f) in all bioassays, regardless of its isotopic composition. The dFe concentrations in F and TF treatments (0.29 ± 0.07 nM) at the end of the bioassays were comparable to concentrations in non-Fe-addition treatments (0.28 ± 0.14 nM, Table S8) for bioassay A1, which was relatively high in Chl *a*. In contrast, bioassay A2 had the most dFe left at the end of the incubation (0.80 ± 0.46 nM for F and TF, compared to 0.11 ± 0.04 nM for C and T), which concurs with the low starting Chl *a* concentration and irradiance intensity. However, since the average dFe concentration in Fe-amended treatments was lower (0.65 ± 0.10 nM) in the middle of the incubation period (day 3; see Fig. 2b), we cannot rule out potential contamination during sampling as a reason for the higher dFe concentrations, notably in the F treatment. For the Weddell Sea bioassays, $d^{57}Fe$ in F and TF treatments declined rapidly with low final concentrations (0.14 ± 0.03 and 0.31 ± 0.17 nM for W1 and W2, respectively) compared to the non-Fe-addition treatments (0.01 ± 0.01 nM $d^{57}Fe$ and below the detection limit for W1 and W2, respectively). Other trace metals were also measured, and dissolved manganese (dMn) drawdown did not differ between treatments (Fig. 2g–j). However, the starting concentrations of dMn were low for W1 and W2 (0.06 ± 0.03 and 0.19, SD < 0.01 nM, compared to 0.76, SD < 0.01, and 1.16 ± 0.01 nM for A1 and A2, respectively).

The dissolved inorganic macronutrients were not limiting phytoplankton growth during the bioassays. Final concentrations were at least 7.2, 0.3 and 37 µM in all bioassays for nitrogen, phosphate and silicate, respectively (Supplement, Fig. S4). Still, there was discernible drawdown of macronutrients by the microbial community during the incubations, except for Amundsen Sea bioassay A2 (Supplement, Tables S10 and S21). Fe addition (both F and TF treatments) had a significant impact on phosphorous drawdown for bioassays A1, W1 and W2 ($p < 0.05$, η^2: 0.53, 0.76 and 0.76 for A1, W1 and W2, respectively, with final phosphorous concentrations being on average 0.45 µM lower for Fe-addition treatments compared to C) and on nitrogen drawdown for bioassays W1 and W2 ($p < 0.004$ and η^2 over 0.75, with final nitrogen concentrations being on average 9.8 µM lower for Fe-addition treatments compared to C). The TF treatment showed stronger drawdowns, especially for Weddell Sea bioassays W1 and W2 (average 0.7-fold change between TF and F treatments for both phosphorus and nitrogen); however there was no significant interaction effect between temperature increase and Fe addition. In contrast, silicate acid concentrations at the end of the incubation period were impacted by the increase in temperature for bioassays A1, A2 and W2 ($p < 0.02$ and η^2 is 0.76 for A1 and W2 and 0.52 for A2; $p = 0.06$ and η^2 is 0.32 for bioassay W1), with T treatments showing on average a 2.4 µM lower silicate concentration compared to the control. Only bioassay W1 showed an effect of Fe addition on silicate drawdown ($p = 0.02$ and η^2 is 0.52), resulting in the TF treatment showing the lowest concentrations on the last day of the incubations (0.8-fold change compared to the control and 0.9-fold change compared to both the T and the F treatments). The ratios of silicate drawdown to nitrogen and to phosphorus were higher in W1 than in W2 (i.e. 1.4 and 18.3 in W1 and 0.7 and 10.5 in W2). Moreover, when dFe was added, the drawdown in these ratios was lower in bioassays A1, W1 and W2 compared to non-Fe treatments (0.86 and 1.02 Si : N and 11.3 and 12.5 Si : P for Fe and non-Fe treatments, respectively, Table S10).

Particulate Fe concentrations (natural pFe for A1, $p^{57}Fe$ for W1 and W2) increased over time for the Fe-addition treatments (Table S21 metadata, Table S8) in all bioassays examined (excluding A2 as particulate metals were not measured there), and pFe concentrations on the last day of incubations were (positively) impacted by Fe addition ($p \leq 0.01$ and $\eta^2 \geq 0.73$ for A1, W1 and W2; final concentrations were 8.01 ± 0.83, 1.09 ± 0.10 and 0.89 ± 0.33 nM for Fe-addition treatments and 4.40 ± 0.21; 0.08 ± 0.02; and 0.09, SD < 0.01 nM, for treatments without Fe addition for A1, W1 and W2, respectively).

To examine potential differences in phytoplankton trace metal stoichiometry in response to Fe addition and/or warming, we calculated the ratio of pFe and other trace metals (pMn, pZn, pCd and pCu) to POP concentrations (Fig. 3, Table S21). The initial lithogenic fraction of particulate trace metals was on average 60 % in the Amundsen Sea compared to 52 % in the Weddell Sea. Particulate Al, and hence the estimated lithogenic particle concentrations, remained in the same range between the start and end of the experiments (Table S20), and thus the lithogenic particles provided a consistent background that did not affect observed changes between treatments. Fe addition significantly increased pFe : POP ratios (natural pFe for A1 and $p^{57}Fe$ for W1 and W2, Table S11) for all bioassays ($p \leq 0.01$ and $\eta^2 \geq 0.73$; average 2.5-fold change for natural pFe : POP (A1) and 13.3-fold change for $p^{57}Fe$: POP in Weddell Sea bioassays for Fe-addition treatments compared to the control). Furthermore, the pMn : POP ratios increased (by 0.33 compared to C) due to Fe addition in bioassay A1 and decreased (by 0.13 compared to C) in W2 ($p < 0.01$ and 0.004 and η^2 is 0.74 and 0.76, respectively). For bioassay W1, neither Fe nor temperature alone had a significant impact

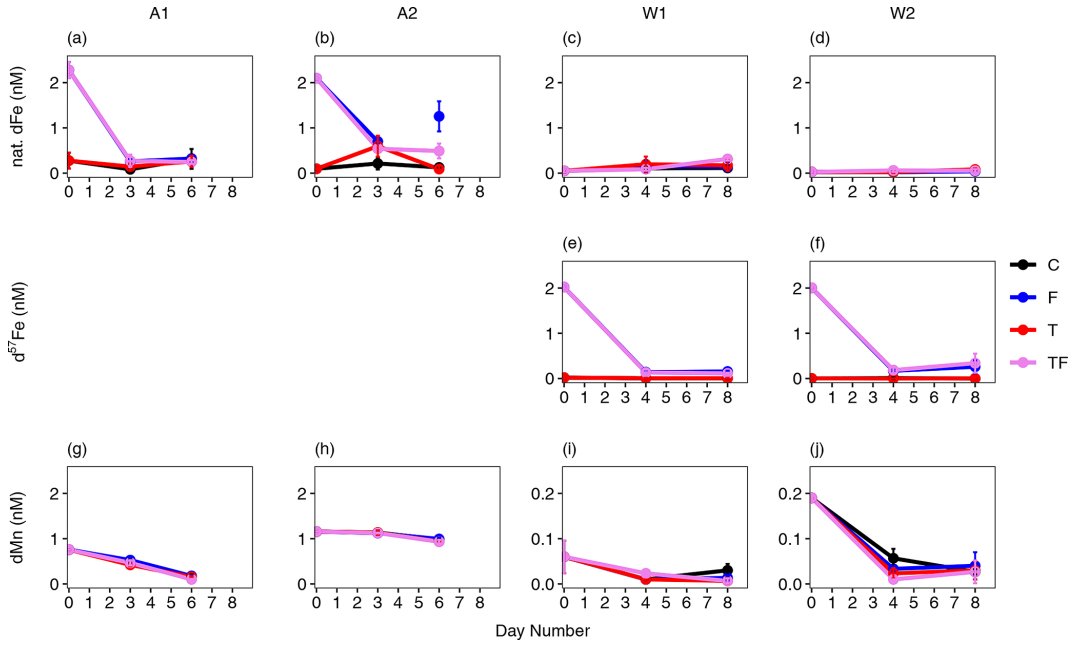

Figure 2. Average concentrations of natural dissolved Fe **(a, b, c, d)**, $d^{57}Fe$ **(e, f)** and dMn **(g, h, i, j)** concentrations for the Amundsen Sea (A1: **a**, **g**; A2: **b**, **h**) and Weddell Sea (W1: **c**, **e**, **i**; W2: **d**, **f**, **j**) bioassays. Amundsen Sea bioassays did not receive ^{57}Fe supplementation. The black line represents the control (C) treatment, the red line the temperature (T) treatment, the blue line the iron (F) treatment, and the pink-purple line the combined temperature and iron treatment (TF). Error bars indicate the standard deviation ($n = 2$ or 3, except for the dFe of bioassay A2 TF treatment on day 3); when they are not visible, they are smaller than the symbol. Bioassay A2 showed a higher dFe concentration on day 6 compared to day 3; we cannot exclude the possibility that this was due to potential contamination, and it was thus treated as an outlier.

on the *p*Mn : POP ratio; however, the combination of both treatments was found to be significant ($p = 0.01$ and η^2 is 0.63), with the TF treatment showing an average 1.4-fold-changed ratio compared to all other treatments. Additionally, the pCd : POP ratio was significantly affected by Fe addition in W1 and W2 ($p < 0.05$ and η^2 is 0.76 and 0.39 for W1 and W2), showing decreased values (by on average 0.12) for Fe-addition treatments compared to the control (Fig. 3o–q); however no effect was seen for bioassay A1. A similar outcome was observed for pZn : POP ratios ($p \leq 0.01$ and η^2 is 0.65 and 0.76 for W1 and W2, respectively, by on average 1.8 compared to C). For pCu : POP ratios, a decrease due to Fe addition was mainly observed in bioassays A1 and W2 ($p < 0.009$ and $\eta^2 \geq 0.73$, by on average 0.16 compared to C), while for bioassay W1, Fe addition caused a notable but not statistically significant effect ($p = 0.09$ and η^2 is 0.32, Fig. 3, by on average 0.23 compared to C).

3.3 Photosynthetic efficiency

Fe addition led to an increase in F_v/F_m for all bioassays (Fig. 4, $p \leq 0.009$ and $\eta^2 > 0.68$ for all bioassays, Table S12), with stronger increases in Weddell Sea compared to Amundsen Sea bioassays (average of 1.42- and 1.14-fold change for Fe-addition (F and TF) versus control treatments for Weddell Sea and Amundsen Sea bioassays, respectively). Towards the end of the incubations of W1 and W2, F_v/F_m decreased slightly again for the Fe-addition treatments (the most for TF, with final F_v/F_m values still being higher than for C and T treatments), coinciding with Fe depletion (Fig. 2).

3.4 POC, Chl *a* and phytoplankton taxonomic community composition

Total Chl *a* concentration at the start of the incubations (Table 1) was highest for bioassay A1 inside the ASP ($3\,\mu g\,L^{-1}$) and lowest for bioassay A2 outside the ASP ($0.4\,\mu g\,L^{-1}$). Of the Weddell Sea bioassays, W1 had the highest Chl *a* starting concentration (1.5 compared to $0.6\,\mu g\,L^{-1}$ for W1 and W2). Starting concentrations of total POC in A1 and W1 were higher than A2 and W2 (384 and $347\,\mu g\,L^{-1}$ compared to 91 and $136\,\mu g\,L^{-1}$, respectively). The POC-to-Chl *a* ratio was lower for A1 (130) than the other bioassays (212–239). Total POC concentrations did not display differences between treatments at the end of the incubations for A1 and A2 (Fig. 5a–d), yet total Chl *a* concentrations exhibited treatment-specific differences for all bioassays (Fig. 5e–h, Table S13). Only bioassays W1 and W2 showed a significant increase in bacterial abundances with Fe addition (final abundance 4.7 ± 0.9, 4.5 ± 0.5 vs. 3.1 ± 1.0 and 4.7 ± 0.6, 5.4 ± 0.2 vs. 4.4 ± 0.1 for F, TF vs. C treatments in W1 and W2, respectively, Table S12). However, bacteria did not

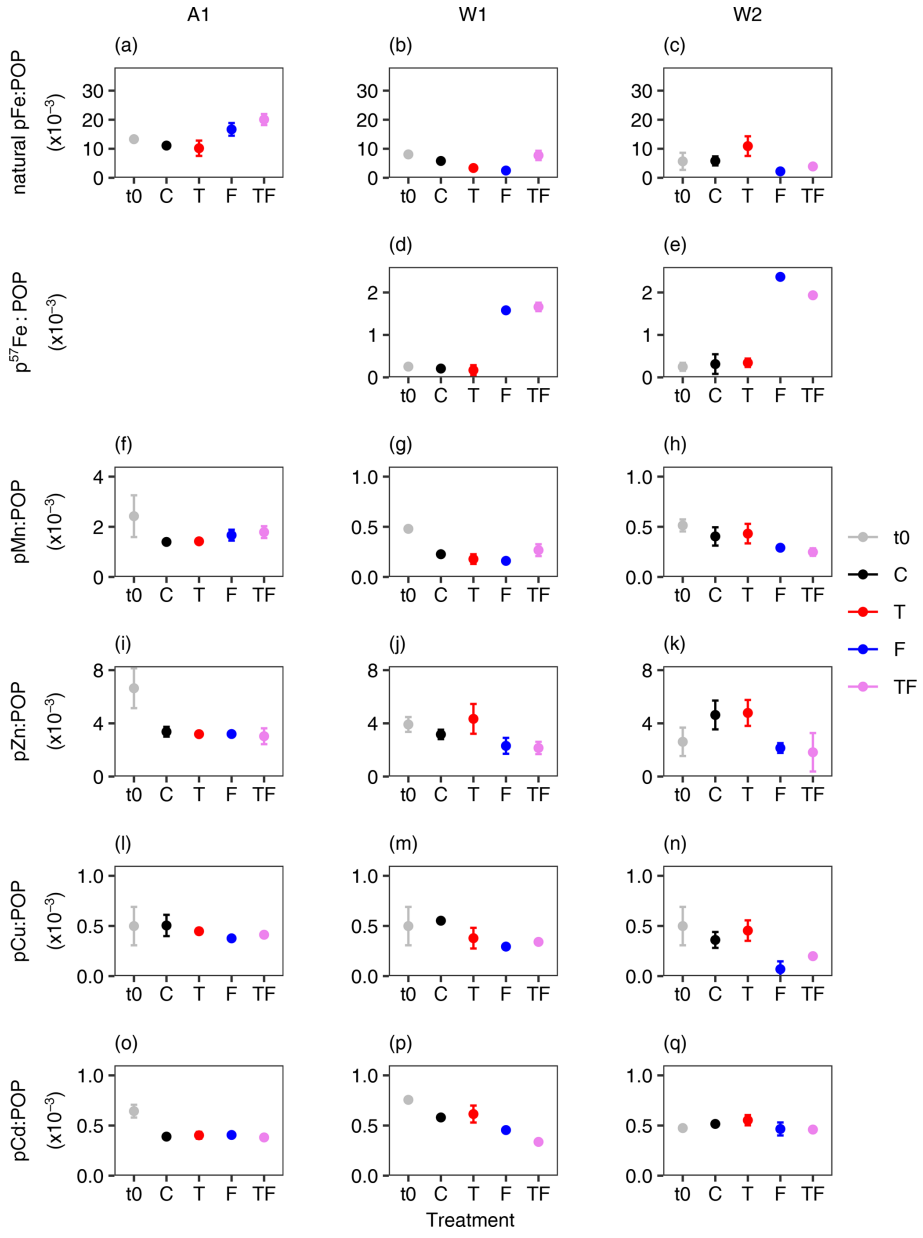

Figure 3. Average ratios ($\times 10^{-3}$, mM : M) of particulate trace metal to particulate organic phosphorus (POP) for Amundsen Sea A1 **(a, f, i, l, o)** and Weddell Sea W1 **(b, d, g, j, m, p)** and W2 **(c, e, h, k, n, q)** bioassays. There are no data available for A2. pFe denotes natural particulate iron, $p^{57}Fe$ denotes particulate iron in the ^{57}Fe form (not added to bioassay A1), pMn denotes particulate manganese, pZn denotes particulate zinc, pCu denotes particulate copper and pCd denotes particulate cadmium. t_0 are starting ratios, whilst ratios for C (control), T (temperature), F (iron) and TF (combination of temperature and iron) were measured on the last day of the incubations (days 6 and 8 for the Amundsen Sea and Weddell Sea bioassays, respectively). Error bars indicate the standard deviation ($n = 2$ or 3), except for the bioassay A1 T treatment for all ratios and bioassay W1 C treatment for the pFe : POP ratio, where $n = 1$. If the error bar is not visible, then it is smaller than the symbol. Please note the different y-axis ranges for manganese-to-POP ratios **(f–h)**.

have a major effect (less than 3 %) on total POC concentrations. Fe addition always positively impacted Chl a concentrations (p is 0.02, 0.005 and 0.006 and η^2 is 0.52, 0.76 and 0.67 for bioassays A1, W1 and W2, respectively; not tested for A2 due to $n = 1$ for all Chl a samples and for W1 C due to $n = 1$); however the effect was stronger in Weddell Sea bioassays (average of 1.6- and 2.9-fold difference for Amundsen Sea and Weddell Sea with Fe addition compared to C). Amundsen Sea bioassays also showed a slight increase in Chl a with increased temperatures. The strongest treatment-specific increases in Chl a concentrations were, however, obtained for the TF treatment in all bioassays, re-

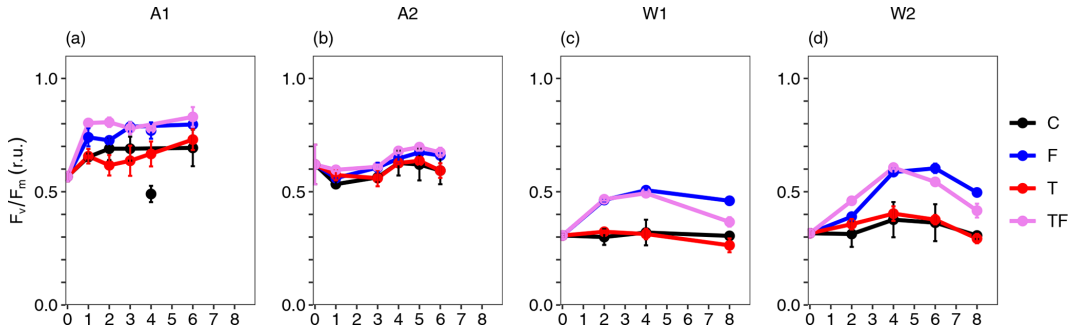

Figure 4. Temporal dynamics of the photosynthetic efficiency (F_v/F_m, relative units) of the phytoplankton for the Amundsen Sea A1 **(a)** and A2 **(b)** and the Weddell Sea W1 **(c)** and W2 **(d)** bioassays. The black line represents the control (C) treatment, the red line the temperature (T) treatment, the blue line the iron (F) treatment, and the pink-purple line the combined temperature and iron (TF) treatment. Averages are of triplicates with error bars representing the standard deviation; if not visible, they are smaller than the symbol. The control treatment of bioassay A1 showed an outlier for F_v/F_m values on day 4, which was excluded.

sulting in an average of 1.7 µg more Chl *a* per litre compared to the F treatment. POC concentrations in W1 and W2 showed similar treatment responses to total Chl *a* in these bioassays.

The TF treatment also caused the strongest increase for the < 20 µm Chl *a* fraction (Fig. 5e–h) for all bioassays, and Fe addition generally had a positive impact on < 20 µm Chl *a* concentrations, with effects being the strongest in both Weddell Sea bioassay W1 and Weddell Sea bioassay W2 (increases of 1.2, 0.2, 0.5 and 0.7 µg L^{-1} for A1, A2, W1 and W2 compared to the control, respectively, with $p = 0.04$ and 0.006 and η^2 being 0.37 and 0.67; A2 and W1 were not tested due to missing replicates). The < 20 µm fraction at the start of the bioassays made up 42 %, 24 % and 65 % of total Chl *a* in A1, W1 and W2, respectively, whereas for bioassay A2, 95 % of the total Chl *a* concentration was < 20 µm. At the end of the bioassays, shares were 42 %, 25 %, 35 % and 70 % for A1, W1, W2 and A2, respectively.

Diatoms dominated the phytoplankton community at the start of A1 and W1 (53 % and 62 % of total Chl *a*), followed by haptophytes (34 % and 27 %; Fig. 5i–l). Bioassay W2 had a comparable share of diatoms and haptophytes (42 % and 46 % of total Chl *a*), whilst the phytoplankton community of A2 was taxonomically most diverse.

Diatoms showed in general a strong response to Fe addition (F and TF treatments) and could be defined as an indicator group for Fe-addition treatments in A1 and W2 ($p < 0.005$). Absolute diatom abundances increased as well with Fe addition, especially for the TF treatment, in bioassays A1 (F and TF treatments, $p = 0.007$) and W2 (TF treatment, $p = 0.02$, Table S21). In bioassay W2, diatoms also showed a higher share for Fe-addition treatments in the < 20 µm fraction ($p < 0.05$), with absolute abundances being higher in the TF treatment for bioassays A1, W1 and W2 ($p < 0.04$) and bioassay W1 also showing higher abundances at the F treatment ($p = 0.04$). The contribution of haptophytes declined (in response to the diatom increase, also in W1 where the diatom response was not significant, $p < 0.007$); however their absolute concentration (in µg Chl *a* L^{-1}; Table S21) did not decline except for the F treatment in bioassay W2 ($p = 0.01$). Both the share ($p = 0.01$) and absolute concentration ($p = 0.04$) of pelagophytes increased with Fe addition in the < 20 µm fraction of bioassay A1. Cryptophyte abundances increased in the total fraction of the TF treatment for A1 and W2 ($p = 0.02$ and 0.01, respectively) and in the < 20 µm fraction for W1 ($p = 0.02$); however their share did not change with treatments.

3.5 Phytoplankton abundances

The total abundances of < 20 µm phytoplankton (Figs. 6 and S5, Table S21) increased with time for all bioassays, and the treatment-specific dynamics largely mimicked the responses observed for the < 20 µm Chl *a* fraction (Fig. 5e–h, Table S12). Bioassay A1 had the highest phytoplankton abundances overall (up to $40\,000 \pm 4000$ cells mL^{-1} for the TF treatment; Fig. 6a) and was dominated by *Phaeocystis antarctica* Phyto 8 (the highest abundances of 37 053 mL^{-1} were observed in the TF treatment; Table S21). Phyto 19 increased in abundance and share (Fig. 6a, Table S14) specifically in the temperature treatments, with net growth rates of 0.40 ± 0.08 d^{-1} and 0.52 ± 0.005 d^{-1} for the T and TF treatments (compared to 0.35 ± 0.11 d^{-1} and 0.30 ± 0.09 d^{-1} for C and F treatments, $p < 0.04$, Table S15) and final abundances of 2800 and 3500 cells mL^{-1} for T and TF (compared to 1700 and 1300 mL^{-1} for C and F, $p < 0.01$). Phyto 3 also showed higher abundance-derived net growth rates with warming (0.33 ± 0.13, 0.32 ± 0.002 and 0.26 ± 0.06 d^{-1} for the T, TF and C treatments, respectively) but with abundances being only significantly higher for the TF treatment (776 ± 37 vs. 542 ± 107 cells mL^{-1} for the TF and C treatments). Phyto 24 was positively impacted by Fe addition; particularly the TF treatment resulted in higher net growth rates and final abundances (i.e. 0.32 ± 0.09 vs. 0.15 ± 0.06 d^{-1} and 595 ± 62 vs. 361 ± 9 cells mL^{-1} for

TF compared to the C treatment; $p < 0.05$). When converted to cellular carbon based on cell volume using 237 and 196.5 fg C μm^{-3} as conversion factors for pico- and nanophytoplankton, respectively (Fig. 6e), the strong positive response of the phytoplankton to the TF treatment was mostly due to this larger-sized Phyto 24 (average diameter of 19 µm, $p = 0.01$) and to a smaller extent Phyto 19 ($p < 0.01$).

Bioassay A2 presented the highest share of picoeukaryotes, especially Phyto 3 (59 % compared to max 18 % in the other bioassays, Fig. 6b). Only a few treatment-specific responses were recorded. Phyto 19 increased somewhat with warming ($p = 0.04$), and Phyto 16 and Phyto 17 showed increased net growth rates with Fe addition (0.31 ± 0.22 and 0.23 ± 0.06, 0.09 ± 0.16 and 0.31 ± 0.06, and 0.30 ± 0.06 and 0.23 ± 0.06 for the F, TF and C treatments of Phyto 16 and Phyto 17, respectively, $p < 0.02$ for both; Tables S14, S16). The phytoplankton populations in W1 were distributed more equally (Fig. 6c), with higher abundances of especially Phyto 16 and Phyto 17 for the Fe-addition treatments ($p < 0.05$, most pronounced for TF, with average abundances of 3103 ± 1290 vs. 948 ± 218 cells mL^{-1} and 2041 ± 572 vs. 1158 ± 216 cells mL^{-1} for Phyto 16 and Phyto 17, respectively, in the TF vs. C treatments, Table S14). Their specific net growth rates were up to 2.2-fold higher for the Fe-addition treatments than the control (0.29 ± 0.02, 0.38 ± 0.10 and 0.20 ± 0.02 and 0.16 ± 0.02, 0.21 ± 0.06 and 0.09 ± 0.02 d^{-1} for the F, TF and C treatments of Phyto 16 and Phyto 17, respectively, Table S17). When expressed in carbon, Phyto 16 was still a recognizable indicator species ($p = 0.03$), but at the same time the larger-sized Phyto 21 (average cell diameter of 10 µm) and diatom groups Phyto 22–Phyto 24 (13–19 µm) showed clear positive responses to Fe addition (Fig. 6g, $p < 0.05$ for all). Net growth rates were largely comparable for these phytoplankton groups: 0.23 ± 0.02, 0.19 ± 0.01, 0.17 ± 0.04 and 0.20 ± 0.05 d^{-1} in the F treatment (and similar net growth rates in the TF treatment) compared to 0.09 ± 0.07, 0.14 ± 0.03, 0.04 ± 0.04 and 0.12 ± 0.02 in the C treatment for Phyto 21–Phyto 24, respectively ($p < 0.03$). Bioassay W2 also showed a distinct shift in favour of Phyto 16 and Phyto 17 (away from Phyto 13) with Fe addition, even early in time (Table S21), for both abundances and cellular carbon (Fig. 6d and h, $p < 0.01$ for all, Table S14). The F treatment net growth rates of Phyto 16, Phyto 17 and Phyto 13 were 0.42 ± 0.02, 0.34 ± 0.03 and 0.21 ± 0.09 d^{-1} (again with similar growth in the TF treatments) compared to 0.20 ± 0.03, 0.17 ± 0.04 and 0.37 ± 0.02 d^{-1} in the C treatment ($p < 0.03$, Table S18). The diatom groups Phyto 23 and Phyto 24 also responded positively to Fe addition with ~2-fold-higher net growth rates than the control (Fig. 6h, $p < 0.01$). Phyto 23 net growth rates were 0.37 ± 0.06 and 0.39 ± 0.04 d^{-1} for F and TF compared to 0.19 ± 0.06 d^{-1} for the C treatment ($p = 0.004$), and Phyto 24 net growth rates were 0.38 ± 0.08 and 0.32 ± 0.05 for F and TF treatments vs. 0.22 ± 0.09 for the C treatment. Phyto 19 was the only phytoplankton population that showed a consistent selective positive response (in share) to warming (and not to Fe addition) in the Amundsen Sea bioassays. The diatom group Phyto 22 increased with temperature in bioassay W2 ($p \leq 0.01$). We refer to Table S21 for less pronounced responses of the other phytoplankton populations. Overall, the response by the larger phytoplankton populations is also illustrated by the higher average cellular biovolumes in the F and TF treatments of W1 and W2 (Fig. S6). The Amundsen Sea bioassays did not show a treatment-specific increase in phytoplankton biovolume. Fe addition had a significant effect on total phytoplankton abundances for Weddell Sea bioassays ($p < 0.02$ and η^2 is 0.56 and 0.74 for W1 and W2, respectively, with Fe addition leading to an average 1.6-fold change compared to C). The GLM we applied (explained deviance: 86 %) indicates an interaction effect of Fe addition and warming ($p = 0.03$ for the interaction and exponentiated coefficient (ec) of 1.13); i.e. Fe addition of 2 nM in combination with a 2 °C temperature increase led to an overall increase in algal abundances of about 28 %. Fe addition (ec: 1.03), temperature increase (ec: 1.11), bioassay and day number ($p < 0.001$ for all; for other statistical parameters, see Table S20) were also significant explanatory factors. The NMDS analysis of the Weddell Sea bioassays (Fig. S7c, d) demonstrated a clear distinction between the Fe-addition treatments and the non-addition treatments after the second day of the incubations. For bioassay W1, the TF and T treatments clustered on the last day of incubation separately from the F and C treatments, respectively. For bioassay W2, the T treatment was also separate on the last day, while the TF and F treatments remained closer together. Bioassays A1 and A2 did not display obvious clustering by treatment, other than time (i.e. separation after day 2).

4 Discussion

4.1 Trace metal and macronutrient dynamics

The pFe concentrations showed the expected significant increase in the Fe-addition treatments for both the Amundsen Sea (natural dFe added) and the Weddell Sea ($d^{57}Fe$ added) bioassays at both temperatures, indicating that the added dFe was indeed taken up and incorporated in the phytoplankton cells. Additionally, in bioassay W2 the final $p^{57}Fe$ in the TF treatment was higher than in the F treatment (1.12 ± 0.11 nM compared to 0.66 ± 0.20 nM), demonstrating enhanced Fe uptake with higher temperatures.

The higher starting concentrations of dFe in the Amundsen Sea compared to the Weddell Sea can be attributed to the Fe input from basal melt (Rignot et al., 2013). Conversely, the naturally low dFe concentrations in the Weddell Sea underscore the area's limited Fe input (e.g. de Baar et al., 1990; Klunder et al., 2011). Fe is needed in nitrate assimilation, and as such uptake of nitrate is coupled to the Fe nutritional status

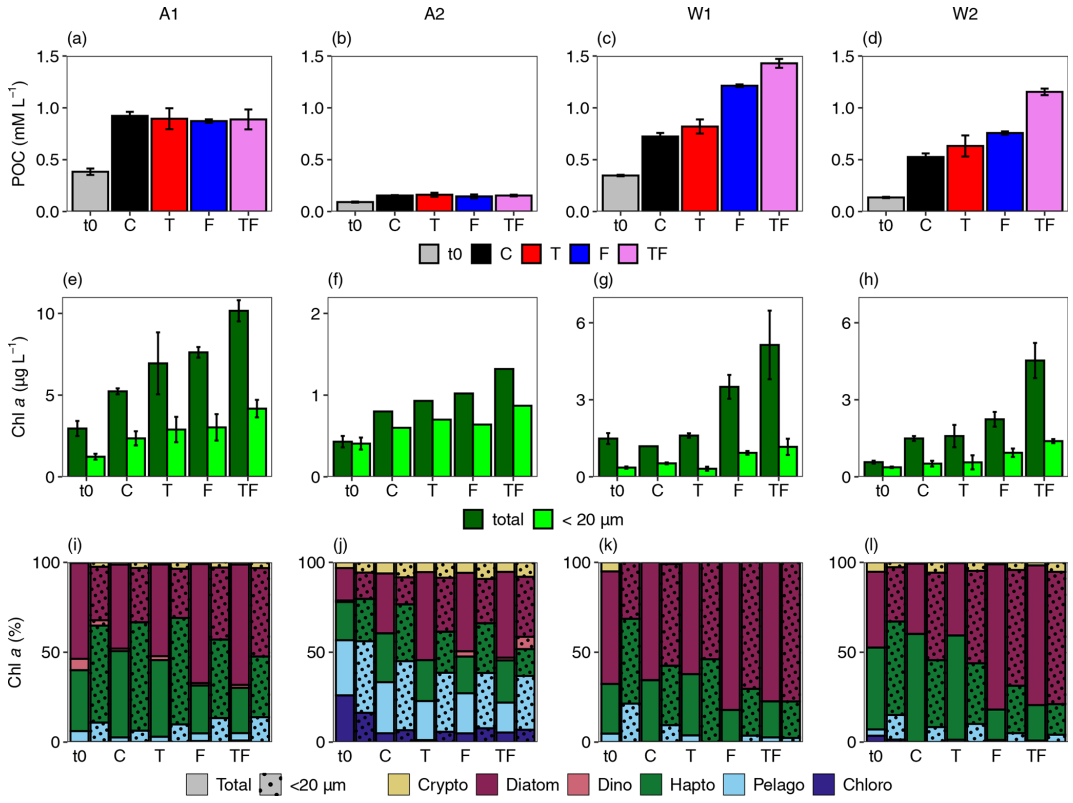

Figure 5. Average concentrations of particulate organic carbon (POC, **a–d**), total and $< 20\,\mu m$ (dotted columns) Chl *a* **(e–h)**, and the taxonomic composition of the phytoplankton community (**i–l**, percentage of total Chl *a*) for the Amundsen Sea A1 **(a, e, i)** and A2 **(b, f, j)**, and the Weddell Sea W1 **(c, g, k)** and W2 **(d, h, l)** bioassays. Error bars represent the standard deviation ($n = 3$ except when no error bar is shown, and then $n = 1$). t_0 denotes the starting conditions, C denotes control, T denotes the temperature treatment, F denotes the iron-addition treatment, and TF denotes the temperature and iron-addition treatment. For **(i)–(l)**, Crypto, Dino, Hapto, Pelago and Chloro stand for cryptophytes, dinophytes, haptophytes, pelagophytes and chlorophytes, respectively. Solid bars represent the total and shaded bars the $< 20\,\mu m$ fraction community composition. Note the differences in the *y* axis for the Chl *a* panels **(e–h)**.

(Schoffman et al., 2016; Milligan and Harrison, 2000). Similarly, diatom cellular silicate-to-nitrogen ratios are known to increase in response to Fe stress (Meyerink et al., 2017). The highest drawdown of the macronutrients typically occurred in the TF treatment, which also showed the largest phytoplankton accumulation (Tables S20, S21). However, whilst dissolved inorganic phosphate and nitrogen drawdown was mostly affected by Fe addition, silicate drawdown in bioassays A1 and W2 was more impacted by temperature. Despite a lower Chl *a* concentration (both total and $< 20\,\mu m$) and lower phytoplankton abundance for the T treatment compared to the TF treatment in these bioassays, the silicate drawdown was comparable. Although Fe stress is reported to cause reduced cellular Chl *a* concentrations compared to Fe-replete conditions (Greene et al., 1992), it is an unlikely cause as the total phytoplankton abundances displayed similar differences between the T and TF treatments compared to $< 20\,\mu m$ Chl *a* concentrations. Instead, higher temperature may have stimulated Si uptake, as reported for the diatom *Pseudo-nitzschia seriata* at temperatures above 0 °C (Stapleford and Smith, 1996). It might also be that the T treatment experienced higher Fe stress than the control, which is also known to increase Si uptake (Meyerink et al., 2017). However, since phytoplankton abundances, F_v/F_m and Chl *a* concentrations were not higher in T treatments compared to the control and since Antarctic phytoplankton may require less Fe at higher temperatures (Jabre and Bertrand, 2020), this is less likely. Bioassay W1 showed the strongest decline in silicate concentrations, with both temperature and Fe affecting silicate drawdown. The relatively high fraction of diatoms (and specifically the large-sized Phyto 20 and Phyto 22–Phyto 24) in bioassay W1 could theoretically have caused the strong silicate drawdown and high ratio of silicate relative to nitrogen (or phosphorus) uptake for all treatments. However, A1 also had high diatom abundances, and over the course of the incubations the concentration of diatoms in W2 became comparable to W1. An alternative explanation may be that Mn stress in W1 (0.06 ± 0.04 vs. 0.19 ± 0 nM in W1 and W2, respectively) enhanced Si uptake, similarly to Fe stress (Hutchins and Bruland, 1998). Increased Si uptake by

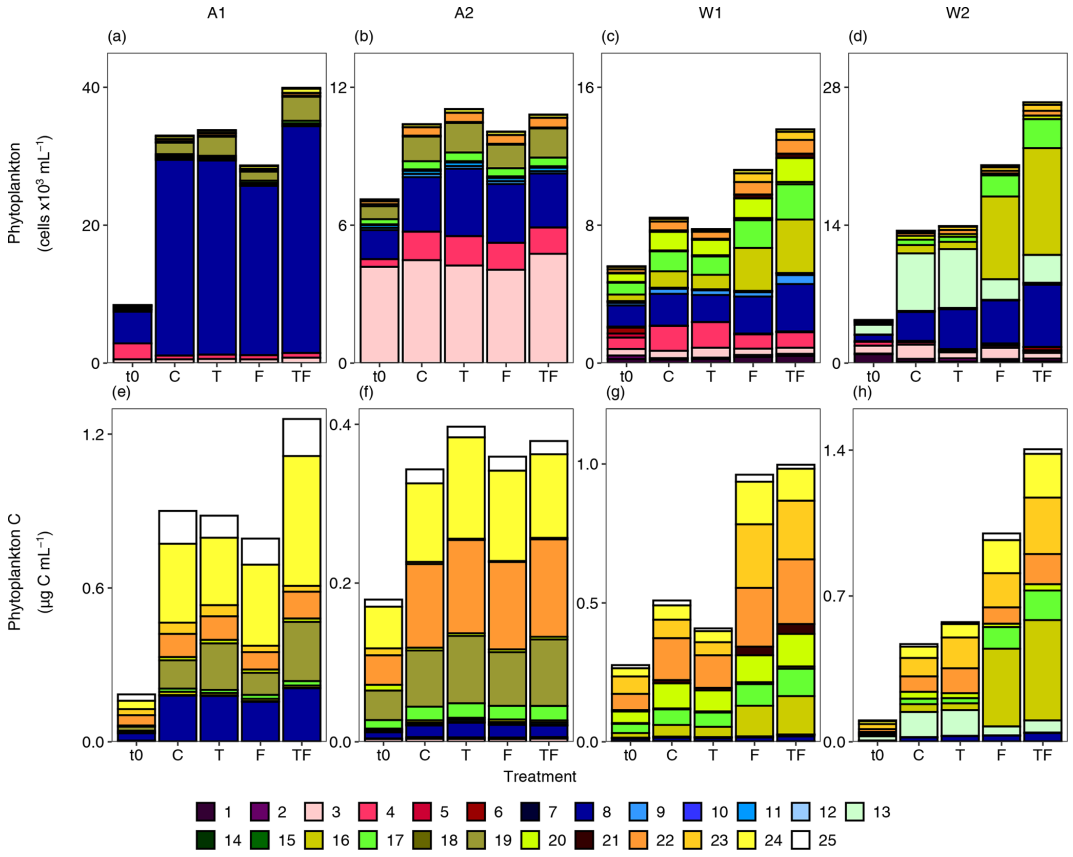

Figure 6. Flow-cytometry-based phytoplankton community composition **(a–d)** and carbon **(e–h)** at the start (t_0) and the end of the bioassay incubations for the different treatments (average of triplicates) for Amundsen Sea bioassays A1 **(a, e)** and A2 **(b, f)** and Weddell Sea bioassays W1 **(c, g)** and W2 **(d, h)**. t_0 denotes the starting conditions, C denotes control, T denotes the temperature treatment, F denotes the iron-addition treatment, and TF denotes the temperature and iron-addition treatment. Phytoplankton groups are sorted by size, with Phyto 1–Phyto 6 $\leq 3\,\mu m$, Phyto 7–Phyto 20 $\leq 10\,\mu m$ and Phyto 21–Phyto 25 $\geq 10\,\mu m$. Phyto 5, Phyto 6, Phyto 7, Phyto 11, Phyto 12 and Phyto 14 are cryptophytes; Phyto 20 and Phyto 22–Phyto 25 are diatoms; and Phyto 8 is *Phaeocystis antarctica*. Note the different scales.

diatoms under a combined Fe and Mn limitation may possibly enhance protection against grazers (Assmy et al., 2013; Ryderheim et al., 2022) and/or enhance sinking to nutrient-richer depths (Waite and Nodder, 2001). Considering an increasing awareness of trace metal co-limitation of phytoplankton growth (Wu et al., 2019; Browning et al., 2021; Balaguer et al., 2022; Burns et al., 2023), we recommend further investigation into these potential interactions and their ecological relevance in future studies.

Dissolved Mn is known to (co-)limit Southern Ocean phytoplankton growth and community composition together with Fe (Browning et al., 2021; Balaguer et al., 2022). Under such conditions, Fe addition alone positively impacts Chl *a* concentrations, phytoplankton abundances and POC concentrations, but a combination of dFe and dMn addition can lead to higher increases in these variables (Pausch et al., 2019; Browning et al., 2021). Nevertheless, dMn-addition effects can often be masked by the effects of Fe addition (Latour et al., 2023), and Fe addition alone can be enough to lead to increases in Chl *a* even in primarily Mn-limited areas (Browning et al., 2021). This fits our results showing increases in Chl *a* concentrations with Fe addition. Net growth rates based on total phytoplankton abundances also showed increases (i.e. 1.5-fold higher (0.20 ± 0.05 vs. $0.12 \pm 0.02\,d^{-1}$) and 1.4-fold higher (0.24 ± 0.01 vs. $0.18 \pm 0.01\,d^{-1}$) for Fe-addition treatments (F and TF) compared to the control for bioassays W1 and W2). The lower starting concentrations of dMn in W1 compared to W2 may have contributed to the 2-fold-lower phytoplankton net growth rates in W1 compared to W2, independent of the treatment. Our data indicate potential dMn and dFe co-limitation in the Weddell Sea already in early summer. Since the requirements for dMn and dFe differ between different phytoplankton groups (Arrigo, 2005; Twining and Baines, 2013; Balaguer et al., 2023), we suggest that the (co-)limitation of dMn and dFe may be affected by phytoplankton community composition. Considering that Mn limitation can be seasonal (Latour et al., 2023), we also urge researchers to study different stages of the phytoplankton bloom period.

4.2 Micronutrient stoichiometry

The observed pFe : POP ratios increased upon the addition of iron (natural pFe for bioassay A1 and $p^{57}Fe$ for bioassays W1 and W2), validating the experimental design and confirming the uptake of added dFe by phytoplankton. For other bio-essential (Mn, Zn, Cu) or bio-active (Cd) metals, the metal : POP ratio is expected to be elevated under Fe stress due to the upregulation of non-specific divalent metal transporters under Fe stress (e.g. Kustka et al., 2007; Lane et al., 2008) or the increased uptake of phosphorous relative to metals under Fe-replete conditions (Cullen et al., 2003). Specifically for Mn, this might also be due to a higher cellular Mn requirement under Fe stress (Peers and Price, 2004). The pMn : POP ratios were indeed higher in the C and T treatments compared to the F and TF treatments of W2, but for W1, no consistent effect of Fe was observed (Fig. 3). In contrast, slightly elevated pMn : POP ratios were observed after Fe addition in A1 (F and TF treatments), matching findings by McCain et al. (2021) and Hawco et al. (2022) showing increased Mn demand in environments with high Fe concentrations. This duality in the pMn : POP ratios is not surprising as not only may Mn demand increase under Fe stress but also it should increase with Fe addition, as both Mn and Fe are required for photosynthesis (Raven, 1990; McCain et al., 2021; Hawco et al., 2022). Hence, in an environment with low dMn concentrations, Fe addition can consequently lead to Mn limitation (e.g. Hawco et al., 2022). Dissolved Mn concentrations at the start of bioassay A1 were relatively high, and indeed pMn : POP ratios increased with Fe addition, while concentrations of dMn decreased during the experiment. However, the low (potentially phytoplankton-growth-limiting) dMn concentrations in Weddell Sea bioassays from the start might have prevented a noticeable positive effect of Fe addition on Mn uptake. The higher biomass and cell abundance after Fe addition in these experiments imply the community had to make do with less Mn per cell compared to the treatments without Fe addition (likely resulting in a relatively low Mn quota despite elevated demand), potentially explaining why there was an increase in the pMn : POP ratios in the C and T treatments of W2, whereas this was not observed in W1 with even lower dMn starting concentrations. Such variation in apparent Mn demand and quotas likely reflects adaptive changes in nutrient uptake and storage mechanisms under nutrient stress but could also be due to different phytoplankton community compositions and/or environmental conditions. For example, Twining et al. (2004) observed elevated pMn : POP ratios in individual diatom cells under iron-deplete conditions relative to iron-replete conditions, whereas the trend was the opposite for autotrophic flagellated cells. However, diatoms were dominant in the F and TF treatments in all experiments, suggesting that other factors besides differences in community composition play a role. Since dMn levels are thought to increase with Fe input (e.g. due to ice shelf melting; Van Manen et al., 2022), we recommend including dMn in future studies examining the effects of global climate change on phytoplankton growth.

Besides Mn, other trace metals are known to have variable ratios with respect to POP under different environmental conditions. For example, cellular Cu requirements increase under Fe limitation (Schoffman et al., 2016), which could explain the higher pCu : POP ratios in the C and T treatments compared to the Fe-addition treatments in all bioassays analysed (Fig. 3). Similarly, the pZn : POP ratios were also elevated in the non-Fe treatments in W1 and W2, akin to the pCd : POP ratios, especially in W1, suggesting higher uptake of metals under Fe limitation as previously suggested (Cunningham and John, 2017). This trend of increased uptake of essential (manganese, zinc, copper) and non-essential metals (cadmium) under dFe limitation underscores the adaptive strategies employed by phytoplankton in navigating nutrient scarcities, emphasizing the complexity of nutrient interactions and their collective impact on phytoplankton ecology under varying environmental conditions (e.g. Cunningham and John, 2017). Due to the importance of nutrient uptake in the Southern Ocean for the stoichiometry of global nutrient distributions, notably at lower latitudes (Sarmiento et al., 2004; Middag et al., 2020), changes in (micro)nutrient consumption in the Southern Ocean can have global ramifications for both productivity and ecosystem structure (Moore et al., 2018), which should be further explored in future (modelling) studies. Future studies underpinning these stoichiometric ratios with molecular measurements (e.g. protein expression patterns) could provide further insight into the processes underlying trace metal uptake and use within phytoplankton.

4.3 Impact of F and T treatments on phytoplankton dynamics

The Weddell Sea bioassays exhibited stronger Chl *a* accumulation, a stronger increase in F_v/F_m and increased phytoplankton abundances in response to Fe addition than the Amundsen Sea bioassays, which is likely due to the lower dFe concentrations (and hence higher degree of Fe limitation for the phytoplankton typical of the Weddell Sea) at the start of the incubations. Indeed, given that the Weddell Sea bioassays were performed early in the productive season, these results imply more severe Fe limitation in the Weddell Sea, whereas any Fe limitation in the Amundsen Sea likely only develops later in the season. Consistent with the lower dFe concentrations was the reduced in situ F_v/F_m of the phytoplankton in W1 and W2, which stayed low for non-Fe-addition treatments throughout the experiments, as it is a common indicator of Fe stress in the Southern Ocean (Greene et al., 1992; Mills et al., 2012; Olson et al., 2000; Jabre and Bertrand, 2020). In addition, the low dMn concentration may have contributed to the low F_v/F_m (Wu et al., 2019). The decrease in F_v/F_m in the F and TF treatments towards the end of the Weddell Sea bioassays seem to indi-

cate that the added Fe had been depleted again to limiting conditions or that Mn became (co-)limiting.

The location from where the seawater for bioassay W1 was taken has similar coordinates to bioassay S54–65 in a study by Viljoen et al. (2018). These authors sampled 3 weeks later (in a different year) and at a comparable depth (30 m vs. 20 m in our study) and found largely similar responses by the phytoplankton to Fe addition; i.e. total Chl *a* increased by $\sim 2\,\mu g\,Chl\,a\,L^{-1}$, and diatoms dominated the phytoplankton community. In contrast to W1 but comparable to our other bioassays, the total Chl *a* concentration in bioassay S54–65 (Viljoen et al., 2018) increased in the control over the duration of the bioassay. The lack of increase in Chl *a* in the control (and T) treatment of W1 might be explained by a lower in situ dFe for W1, indicating a stronger limitation of dFe. At the same time, POC (and $< 20\,\mu m$ Chl *a*) concentrations showed an increase over time in the control treatment of bioassay W1. Moreover, bioassay W2, with even lower starting concentrations of dFe, showed an increase in Chl *a* over time for the control. Given the lowest dMn concentrations in W1, it might be that dMn and not (only) dFe was limiting the production of reaction centres (Raven et al., 1990), resulting in Chl *a* concentrations not increasing. Given the increased requirement for Mn under low-Fe conditions (Peers and Price, 2004), Fe addition may have relieved Mn limitation in the Fe-addition treatments slightly, resulting in the observed increase in Chl *a* in those treatments. While for the Weddell Sea bioassays, the POC concentrations followed comparable responses to total Chl *a* upon Fe addition (Fig. 5), the POC concentrations in the Amundsen Sea bioassays did not. The relatively low Chl *a* : POC ratios in the Weddell Sea bioassays (average over all treatments 0.003 ± 0.003 vs. 0.008 ± 0.002 for the Amundsen Sea bioassays) may indicate stronger Fe limitation, since Fe-limited cells are known to have a lower Chl *a* : POC ratio compared to non-limited cells (Moore et al., 2007). Alternatively, acclimation to the lower irradiance during the incubations of A1 and A2 led to the higher Chl *a* : POC ratios at the end of incubations (Laws and Bannister, 1980; Geider, 1987; Geider et al., 1998; Wang et al., 2009). Despite the low light intensities in Amundsen Sea bioassays, Chl *a* concentrations and phytoplankton abundances in the control treatment increased over time (especially in A1, net growth rate based on total abundances of $0.25 \pm 0.03\,d^{-1}$), which indicates that the phytoplankton communities were adapted to low light. Low-light conditions are common for Amundsen Sea phytoplankton (Schofield et al., 2015; Park et al., 2017), but still, the very low irradiance in A2 seemed to have limited growth ($0.09 \pm 0.01\,d^{-1}$), as also illustrated by incomplete depletion of the dFe added (after 6 d of incubation). The high initial F_v/F_m values suggest that the phytoplankton may not have been limited by dFe (under these low-light conditions) and would only require more dFe once light intensities increased again (Strzepek et al., 2019; Vives et al., 2022; Latour et al., 2024). The small increase in F_v/F_m in the Fe-addition treatments may suggest growth became dFe-limited during the incubation (Fe addition did show a significant effect on F_v/F_m on the last day of the incubations), despite the light conditions remaining low. Considering diatoms to be the taxonomic group that responded most to Fe additions (Noiri et al., 2005; Feng et al., 2010; Hinz et al., 2012; Mills et al., 2012; Zhu et al., 2016), the low proportion of diatoms at the start of A2 may also have delayed a measurable effect of Fe addition.

Although earlier studies reported positive responses of phytoplankton to Fe addition under low-light conditions (Viljoen et al., 2018; Alderkamp et al., 2019), the light intensities used for the low-light treatment in those studies were still relatively high (i.e. 15 and 30 µmol quanta $m^{-2}\,s^{-1}$) and well above those in A1 and A2 (average of 3.4 and 1.5 µmol quanta $m^{-2}\,s^{-1}$). In addition to higher light levels, the lower initial dFe concentrations in the Ross Sea study (Alderkamp et al., 2019) compared to our study indicate stronger Fe limitation and subsequently a stronger response to Fe addition. A recent study on Southern Ocean deep-chlorophyll-maximum phytoplankton responses to Fe addition (Latour et al., 2024) reported a Chl *a* increase at low light intensities (similar to our Amundsen Sea bioassays) and no change in POC (similar to bioassay A2) until light levels increased. This supports our suggestion that the low-light condition in A2 was a determining factor for the lack of a response to Fe addition.

Future light conditions in the Southern Ocean will vary for the different regions; e.g. lower sea ice coverage may enhance light availability (Leung et al., 2015; Petrou et al., 2016; Krumhardt et al., 2022), whereas increased cloud coverage in the Antarctic Circumpolar Current region would reduce it (Grise et al., 2013; Kelleher and Grise, 2022; Krumhardt et al., 2022). Moreover, there are conflicting reports about whether mixed-layer depths will increase (Leung et al., 2015) or decrease (Krumhardt et al., 2022), which directly impacts light conditions for the phytoplankton. Our results from the low-light bioassay A2, showing only a small effect of Fe on phytoplankton, suggest that in regions or periods with low light, Fe increase will not drastically stimulate phytoplankton growth. This highlights the importance of including light availability in Southern Ocean ecosystem (modelling) predictions.

Temperature alone showed a limited effect on phytoplankton, with only three phytoplankton groups (Phyto 3, Phyto 19 and diatom group Phyto 22) increasing in abundances and only Phyto 19 showing a consistent effect. Still, these groups represent pico-sized as well as larger phytoplankton (2, 8.1 and 13.3 µm diameter). Earlier studies also showed temperature to have only a limited effect on (natural) phytoplankton communities (Rose et al., 2009). Indirect effects of warming (e.g. locally high ice-melt-induced freshening, dFe increase) will likely have larger impacts on phytoplankton community compositions. Ice-melt-induced freshening has already led to a shift from diatom-dominated to cryptophyte-

and flagellate-dominated communities in the western Antarctic Peninsula region (reviewed by Deppeler and Davidson 2017), and increased dFe concentrations will affect phytoplankton community composition even more so when combined with temperature increases (this study; Rose et al., 2009). Furthermore, the availability of dFe is likely changing due to changes in sources (see the Introduction) but is also influenced by siderophore production (reviewed by Gledhill and Buck, 2012), but warming of the Southern Ocean does not seem to have a direct effect (Sinha et al., 2019). Warming likely increases the growth rates of siderophore-producing bacteria (Sinha et al., 2019), but this may be countered by reduced siderophore production due to ocean acidification (Sinha et al., 2019). Overall, predictions about future conditions and their consequences are complex and have large uncertainty, but it seems likely that conditions will be temporally and spatially heterogenous with varying changes in temperature and availability of Fe (and light). For example, while the warming of surface water in the Amundsen Sea has already been observed, Weddell Sea surface temperatures for the deep basin seem relatively stable at the moment, with significant warming only below 700 m (Strass et al., 2020). However, upwelling of this warm water leads to local temperature increases in notably coastal regions (Darelius et al., 2023), potentially increasing future temperatures by over 2 °C in troughs that connect the open ocean to ice shelves (Teske et al., 2024), increasing not only temperatures but likely also glacial-melt-derived Fe supply. This makes it prudent to assess not only the individual but also the combined effects of increasing Fe and temperature, as discussed in the next section.

4.4 Enhanced responses to Fe with warming

Fe addition led to an overall positive response of Chl *a* concentrations, phytoplankton photophysiology and growth but more so when combined with the ecologically relevant increase in temperature. The increase in phytoplankton abundances was especially distinct for Weddell Sea bioassays. GLM analysis revealed that temperature alone was a significant factor for total phytoplankton abundances; however, more specifically, only Phyto 3, Phyto 19 and Phyto 22 abundances displayed significant positive responses to temperature alone (T treatment). The 2 °C warming alone was thus not a major driver of phytoplankton net growth in our bioassays but accelerated and enhanced Fe-addition responses (significant interaction effect for iron addition and temperature increase on total phytoplankton abundances). The enhanced response to Fe with temperature was especially distinct for bioassay W2 (average 1.61-fold change in total phytoplankton abundances in the TF treatment compared to both the F and the T treatments; W1 showed a 1.48-fold average change). Despite low light levels, this was also seen in Amundsen Sea bioassay A1, albeit to a lower extent (average 1.29-fold change in the TF treatment compared to both F and T treatments). Larger-sized (> 20 µm) diatoms were mainly responsible for the Chl *a* accumulation, which is consistent with previous studies (Noiri et al., 2005; Feng et al., 2010; Hinz et al., 2012; Mills et al., 2012; Zhu et al., 2016) and supports the general consensus that especially large phytoplankton show enhanced growth upon Fe addition due to their lower surface-to-volume ratio (Scharek et al., 1997). However, the (slightly) smaller diatom groups Phyto 23 and Phyto 24 (average cell diameter of 15 and 19 µm, respectively) also responded positively to the combination of Fe and temperature. Diatom group Phyto 24 was even the main phytoplankton population responsible for the increase in the < 20 µm Chl *a* fraction of the TF treatment in A1. The NMDS analysis based on < 20 µm phytoplankton abundances showed clustering for W1 and W2 driven by Fe addition and temperature, indicating that smaller-sized phytoplankton also display positive responses. This is supported by increased < 20 µm Chl *a* concentrations and the 2.2-fold change in cellular carbon of < 20 µm phytoplankton in F and TF treatments in the Weddell Sea bioassays (compared to the C and T treatments). Specifically, we recorded distinct abundance increases in the small 7 µm groups Phyto 16 and Phyto 17 in the F and TF treatments of W2. *Phaeocystis antarctica* (Phyto 8; 3.7 µm) showed higher net growth rates for Fe-addition treatments in both bioassay W1 and bioassay W2, but the effect was not very apparent, and overall, *P. antarctica* seems to handle the other treatments consistently well. Rose et al. (2009) and Zhu et al. (2016) also found diatoms to be preferentially stimulated by Fe addition and/or temperature over *P. antarctica*, which was also found in a broader context where *P. antarctica* dominated under low-Fe conditions, whilst diatoms dominated in regions with higher Fe concentrations (Arrigo et al., 2017). In contrast, Andrew et al. (2019) found comparable growth rates for *P. antarctica* and several diatom cultures (tested under Fe-addition and warming treatments). Similarly to our study, they found the highest growth for the combined Fe-addition and warming treatment for most species. Since diatoms tended to increase most strongly with Fe addition, it can be speculated that phytoplankton community compositions shift towards more diatoms with increases in Fe concentrations; however other biogeochemical factors are also important to consider. The positive phytoplankton growth responses were population-specific, and Phyto 13 (5.5 µm) in W2 even showed reduced abundances for the F and TF treatments, underscoring the multifaceted factors controlling phytoplankton dynamics and emphasizing the importance of understanding how trace metal concentrations and climate change together influence the marine ecosystems in the Southern Ocean.

Alterations in phytoplankton community composition and cell size, as observed in our experiments, will directly affect top-down control by (microzooplankton) grazers and viral infection and consequently trophic transfer efficiency (Eich et al., 2022; Biggs et al., 2021). Not only will the flow of organic carbon through the food web be affected by the differ-

ent phytoplankton mortality, but also the flux of organic carbon to deeper layers of the ocean (biological carbon pump) depends on the phytoplankton community composition, cell size and type of loss factor. Since the seawater was not filtered before distribution to the Cubitainers to reduce contamination risk, there is a chance (although small; Voronina et al., 1994) that large grazers were introduced into the incubations. We did not specifically sample for large grazers but did not notice any on the filters for Chl *a* and POC. Large grazers can be expected to graze on larger phytoplankton (Hansen et al., 1994), thereby reducing phytoplankton net growth. This would be most noticeable for the F and TF treatments, given the positive response of larger phytoplankton to Fe addition. Our results would then have underestimated the effect of Fe enrichment. Moreover, grazing would likely be enhanced with temperature (e.g. Lewandowska and Sommer, 2010; Karakuş et al., 2022), further reducing (and underestimating) net growth rates of larger phytoplankton specifically in the TF treatment. Also, microzooplankton grazing rates are known to increase with temperature (Chen et al., 2012; Caron and Hutchins, 2013), and even viral lysis may occur faster at higher temperature (Maat et al., 2017). This may partially explain the small effect of warming in the bioassays. Besides temperature, Fe availability has been reported to affect algal virus production and infectivity (Slagter et al., 2016; Kranzler et al., 2021). Changes observed in our experiments might thus have also been affected by temperature and/or dFe-related changes in loss factors affecting specific phytoplankton groups.

5 Conclusions

Our study stands out in that it has combined trace metal chemistry and biology, Chl *a*, and population abundance to examine co-effects using natural Antarctic phytoplankton communities at environmentally realistic Fe concentrations (+2 nM) and a predicted (2 °C) temperature increase (Boyd et al., 2015; Jabre et al., 2021; Andrew et al., 2022). Bioassay incubations were performed under trace-metal-clean conditions (the entire duration) and with temperature remaining stable over the course of incubations (maximum fluctuation in temperature of ± 0.3 °C). We stress the importance of trace-metal-clean working conditions to avoid inadvertently assigning Fe-addition effects on phytoplankton to temperature when working in low-Fe regions (i.e. the Southern Ocean), but also in other (open) ocean regions, availability of bio-essential metals is an important factor affecting primary productivity, and hence trace-metal-clean working conditions are recommended for bioassay experiments (Browning and Moore, 2023). The differences we found between the F and TF treatments may have been assigned to temperature alone under non-trace-metal-clean working conditions (as Fe would inadvertently have been introduced), whilst our results show that temperature alone did not have a (major) effect. Our data also show the importance of considering other regional and/or seasonal factors that potentially limit phytoplankton growth, such as light availability (limiting light conditions in bioassay A2) and dMn availability (potentially limiting in W1), when studying the effect of future climate on Southern Ocean phytoplankton. Additionally, our data indicate a trend of increased uptake of trace metals under dFe limitation, suggesting that there are many adaptive strategies employed by phytoplankton in navigating nutrient scarcities under varying environmental conditions, with potential impacts on the stoichiometry of global (micro)nutrient distributions due to the central role of the Southern Ocean. In general, the addition of Fe was the primary factor for observed stimulatory effects, with temperature enhancing the effects of dFe. In particular, large diatoms benefitted from Fe addition, although several smaller-sized phytoplankton populations showed enhanced abundances upon Fe addition. Climate change is predicted to lead to a shift towards smaller phytoplankton (Deppeler and Davidson, 2017; Krumhardt et al., 2022). Our study shows, however, that enhanced Fe input counteracts this warming-induced shift, assuming macronutrients will not become limiting. Given that the intensity of the observed effects varied between the experiments with distinctly different phytoplankton communities, this study emphasizes the need for studying diverse regions of the Southern Ocean and performing multiple bioassays over the productive season to better understand and predict potential future changes, especially as future changes in Fe availability are region-specific (Tagliabue et al., 2016; Van Manen et al., 2022). The Southern Ocean biogeochemical cycling and ecosystems dynamics are complex and need to be better studied in field and modelling studies. The current study underlines the need for assessing consequences of near-future temperature changes at environmentally relevant dFe concentrations.

Data availability. All data presented in this paper (nutrients, trace metals, phytoplankton abundances, photosynthetic efficiencies, Chl *a* concentrations, pigment-based community composition, particulate organic carbon and particulate organic phosphate) are included in this published article and are available at https://doi.org/10.25850/nioz/7b.b.hh (Brussaard et al., 2024).

Supplement. The supplement related to this article is available online at: https://doi.org/10.5194/bg-21-4637-2024-supplement.

Author contributions. RM and CPDB conceptualized the study. CE, MvM, EB, SBEHP, HT, IA, JSPM and RM conducted the fieldwork under the lead of RM; JJ analysed the nutrient samples for the Amundsen Sea bioassays; WHvdP analysed the pigment samples and conducted the CHEMTAX analysis; CE and MvM wrote the original draft; CPDB and RM edited the paper; and EMB, LJJ and

JSPM contributed to the discussion. All authors contributed to commenting on the paper.

Competing interests. The contact author has declared that none of the authors has any competing interests.

Disclaimer. Publisher's note: Copernicus Publications remains neutral with regard to jurisdictional claims made in the text, published maps, institutional affiliations, or any other geographical representation in this paper. While Copernicus Publications makes every effort to include appropriate place names, the final responsibility lies with the authors.

Acknowledgements. We would like to thank the captains and crews of both R/V *Araon* and R/V *Polarstern*, as well as the expedition leaders SangHoon Lee and Olaf Boebel and all other expedition participants. Furthermore, we would like to thank John Seccombe from Aquahort for his support in conceiving and building the heat pumps as well as his remote support during the expeditions and Sharyn Ossebaar for nutrient measurements aboard R/V *Polarstern*. We thank Sven Ober and all colleagues from NIOZ National Marine Facilities (NMF) for the preparation of the Titan sampling system during the expeditions, as well as for building the incubators and helping in the expedition preparation. We are also grateful to Bob Kosters (NIOZ) for his assistance with the incubators, ensuring they maintained the correct temperature throughout our study; Patrick Laan (NIOZ) for helping with the ICP-MS analyses; Flora Wille (NIOZ) for helping with the particulate metal analysis; and Piet ter Schure and his team (DMT Marine Equipment) for supplying a winch system at the last minute for the Titan sampling system used on R/V *Araon*.

Financial support. This work was part of the FePhyrus project (ALWPP.2016.020), which was supported by the Netherlands Polar Programme (NPP), with financial aid from the Dutch Research Council (NWO). Mathijs van Manen was supported by the Utrecht University–NIOZ collaboration. The ANA08B expedition was supported by the Korea Polar Research Institute, grant KOPRI PE24110. The PS117 expedition was supported by the auxiliary use proposal AWI_PS117_02. Erin M. Bertrand was supported by an NSERC Canada Research Chair and the Simons Foundation, grant 504183.

Review statement. This paper was edited by Emilio Marañón and reviewed by three anonymous referees.

References

Aflenzer, H., Hoffmann, L., Holmes, T., Wuttig, K., Genovese, C., and Bowie, A. R.: Effect of dissolved iron (II) and temperature on growth of the Southern Ocean phytoplankton species *Fragilariopsis cylindrus* and *Phaeocystis antarctica* , Polar Biol., 46, 1163–1173, https://doi.org/10.1007/s00300-023-03191-z, 2023.

Alderkamp, A.-C., Van Dijken, G.-L., Lowry, K. E., Connelly, T. L., Lagerström, M., Sherrell, R. M., Haskins, C., Rogalsky, E., Schofield, O., Stammerjohn, S. E., Yager, P. L., and Arrigo, K. R.: Fe availability drives phytoplankton photosynthesis rates during spring bloom in the Amundsen Sea Polynya, Antarctica, Elementa, 3, 43, https://doi.org/10.12952/journal.elementa.000043, 2015.

Alderkamp, A.-C., Van Dijken, G. L., Lowry, K. E., Lewis, K. M., Joy-Warren, H. L., Van De Poll, W., Laan, P., Gerringa, L., Delmont, T. O., Jenkins, B. D., and Arrigo, K. R.: Effects of iron and light availability on phytoplankton photosynthetic properties in the Ross Sea, Mar. Ecol. Prog. Ser., 621, 33–50, https://doi.org/10.3354/meps13000, 2019.

Alfred-Wegener-Institut Helmholtz-Zentrum für Polar- und Meeresforschung: Polar Research and Supply Vessel POLARSTERN Operated by the Alfred-Wegener-Institute, Journal of large-scale research facilities, 3, A119, https://doi.org/10.17815/jlsrf-3-163, 2017.

Andrew, S. M., Morell, H. T., Strzepek, R. F., Boyd, P. W., and Ellwood, M. J.: Iron Availability Influences the Tolerance of Southern Ocean Phytoplankton to Warming and Elevated Irradiance, Front. Mar. Sci., 6, 681, https://doi.org/10.3389/fmars.2019.00681, 2019.

Annett, A. L., Skiba, M., Henley, S. F., Venables, H. J., Meredith, M. P., Statham, P. J., and Ganeshram, R. S.: Comparative roles of upwelling and glacial iron sources in Ryder Bay, coastal western Antarctic Peninsula, Mar. Chem., 176, 21–33, 2015.

Arrigo, K. R.: Marine microorganisms and global nutrient cycles, Nature, 437, 349–355, https://doi.org/10.1038/nature04159, 2005.

Arrigo, K. R. and Van Dijken, G. L.: Phytoplankton dynamics within 37 Antarctic coastal polynya systems, J. Geophys. Res.-Ocean., 108, 3271, https://doi.org/10.1029/2002JC001739, 2003.

Arrigo, K. R., Lowry, K. E., and van Dijken, G. L.: Annual changes in sea ice and phytoplankton in polynyas of the Amundsen Sea, Antarctica, Deep-Sea Res. Pt. II, 71, 5–15, 2012.

Arrigo, K. R., Van Dijken, G. L., Alderkamp, A., Erickson, Z. K., Lewis, K. M., Lowry, K. E., Joy-Warren, H. L., Middag, R., Nash-Arrigo, J. E., Selz, V., and Van De Poll, W.: Early Spring Phytoplankton Dynamics in the Western Antarctic Peninsula, J. Geophys. Res-Ocean., 122, 9350–9369, https://doi.org/10.1002/2017JC013281, 2017.

Assmy, P., Smetacek, V., Montresor, M., Klaas, C., Henjes, J., Strass, V. H., Arrieta, J. M., Bathmann, U., Berg, G. M., and Breitbarth, E.: Thick-shelled, grazer-protected diatoms decouple ocean carbon and silicon cycles in the iron-limited Antarctic Circumpolar Current, P. Natl. Acad. Sci. USA, 110, 20633–20638, 2013.

Balaguer, J., Koch, F., Hassler, C., and Trimborn, S.: Iron and manganese co-limit the growth of two phytoplankton groups dominant at two locations of the Drake Passage, Commun. Biol., 5, 207, https://doi.org/10.1038/s42003-022-03148-8, 2022.

Balaguer, J., Thoms, S., and Trimborn, S.: The physiological response of an Antarctic key phytoplankton species to low iron and manganese concentrations, Limnol. Oceanogr., 68, 2153–2166, https://doi.org/10.1002/lno.12412, 2023.

Basterretxea, G., Font-Muñoz, J. S., Hernández-Carrasco, I., and Sañudo-Wilhelmy, S. A.: Global variability of high-nutrient low-

chlorophyll regions using neural networks and wavelet coherence analysis, Ocean Sci., 19, 973–990, https://doi.org/10.5194/os-19-973-2023, 2023.

Bazzani, E., Lauritano, C., and Saggiomo, M.: Southern Ocean Iron Limitation of Primary Production between Past Knowledge and Future Projections, J. Mar. Sci. Eng., 11, 272, https://doi.org/10.3390/jmse11020272, 2023.

Bertrand, E. M., Saito, M. A., Lee, P. A., Dunbar, R. B., Sedwick, P. N., Ditullio, G. R.: Iron limitation of a springtime bacterial and phytoplankton community in the Ross Sea: Implications for vitamin B12 nutrition, Front. Microbiol., 2, 160, 2011.

Biggs, T. E., Alvarez-Fernandez, S., Evans, C., Mojica, K. D., Rozema, P. D., Venables, H. J., Pond, D. W., and Brussaard, C. P.: Antarctic phytoplankton community composition and size structure: importance of ice type and temperature as regulatory factors, Polar Biol., 42, 1997–2015, 2019.

Biggs, T. E., Huisman, J., and Brussaard, C. P.: Viral lysis modifies seasonal phytoplankton dynamics and carbon flow in the Southern Ocean, ISME J., 15, 3615–3622, 2021.

Boyd, P. W.: The role of iron in the biogeochemistry of the Southern Ocean and equatorial Pacific: a comparison of in situ iron enrichments, Deep-Sea Res. Pt. II, 49, 1803–1821, 2002.

Boyd, P. W., Arrigo, K. R., Strzepek, R., and Van Dijken, G. L.: Mapping phytoplankton iron utilization: Insights into Southern Ocean supply mechanisms, J. Geophys. Res.-Ocean., 117, C06009, https://doi.org/10.1029/2011JC007726, 2012.

Boyd, P. W., Strzepek, R. F., Ellwood, M. J., Hutchins, D. A., Nodder, S. D., Twining, B. S., and Wilhelm, S. W.: Why are biotic iron pools uniform across high- and low-iron pelagic ecosystems?, Global Biogeochem. Cy., 29, 1028–1043, https://doi.org/10.1002/2014GB005014, 2015.

Bronselaer, B., Russell, J. L., Winton, M., Williams, N. L., Key, R. M., Dunne, J. P., Feely, R. A., Johnson, K. S., and Sarmiento, J. L.: Importance of wind and meltwater for observed chemical and physical changes in the Southern Ocean, Nat. Geosci., 13, 35–42, https://doi.org/10.1038/s41561-019-0502-8, 2020.

Browning, T. J., Achterberg, E. P., Engel, A., and Mawji, E.: Manganese co-limitation of phytoplankton growth and major nutrient drawdown in the Southern Ocean, Nat. Commun., 12, 884, https://doi.org/10.1038/s41467-021-21122-6, 2021.

Brussaard, C., Middag, R., Eich, C., and van Manen, M.: Temperature-enhanced effects of iron on Southern Ocean phytoplankton – associated data, NIOZ [data set], https://doi.org/10.25850/nioz/7b.b.hh, 2024.

Buesseler, K. O., Boyd, P. W., Black, E. E., and Siegel, D. A.: Metrics that matter for assessing the ocean biological carbon pump, P. Natl. Acad. Sci. USA, 117, 9679–9687, https://doi.org/10.1073/pnas.1918114117, 2020.

Burns, S. M., Bundy, R. M., Abbott, W., Abdala, Z., Sterling, A. R., Chappell, P. D., Jenkins, B. D., and Buck, K. N.: Interactions of bioactive trace metals in shipboard Southern Ocean incubation experiments, Limnol. Oceanogr., 68, 525–543, https://doi.org/10.1002/lno.12290, 2023.

Caron, D. A. and Hutchins, D. A.: The effects of changing climate on microzooplankton grazing and community structure: drivers, predictions and knowledge gaps, J. Plank. Res., 35, 235–252, https://doi.org/10.1093/plankt/fbs091, 2013.

Chen, B., Landry, M. R., Huang, B., and Liu, H.: Does warming enhance the effect of microzooplankton grazing on marine phytoplankton in the ocean?, Limnol. Oceanogr., 57, 519–526, 2012.

Cullen, J. T., Chase, Z., Coale, K. H., Fitzwater, S. E., and Sherrell, R. M.: Effect of iron limitation on the cadmium to phosphorus ratio of natural phytoplankton assemblages from the Southern Ocean, Limnol. Oceanogr., 48, 1079–1087, https://doi.org/10.4319/lo.2003.48.3.1079, 2003.

Cunningham, B. R. and John, S. G.: The effect of iron limitation on cyanobacteria major nutrient and trace element stoichiometry, Limnol. Oceanogr., 62, 846–858, https://doi.org/10.1002/lno.10484, 2017.

Cutter, G., Casciotti, K., Croot, P., Geibert, W., Heimbürger, L.-E., Lohan, M., Planquette, H., and van de Flierdt, T.: Sampling and Sample-handling Protocols for GEOTRACES Cruises, Version 3, GEOTRACES International Project Office, https://doi.org/10.25607/OBP-2, 2017.

Darelius, E., Daae, K., Dundas, V., Fer, I., Hellmer, H. H., Janout, M., Nicholls, K. W., Sallée, J.-B., and Østerhus, S.: Observational evidence for on-shelf heat transport driven by dense water export in the Weddell Sea, Nat. Commun., 14, 1022, https://doi.org/10.1038/s41467-023-36580-3, 2023.

de Baar, H. J., Buma, A. G., Nolting, R. F., Cadée, G. C., Jacques, G., and Tréguer, P. J.: On iron limitation of the Southern Ocean: experimental observations in the Weddell and Scotia Seas, Mar. Ecol. Prog. Ser., 65, 105–122, http://www.jstor.org/stable/24846120 (last access: 30 September 2024), 1990.

De Baar, H. J. W., Boyd, P. W., Coale, K. H., Landry, M. R., Tsuda, A., Assmy, P., Bakker, D. C. E., Bozec, Y., Barber, R. T., Brzezinski, M. A., Buesseler, K. O., Boyé, M., Croot, P. L., Gervais, F., Gorbunov, M. Y., Harrison, P. J., Hiscock, W. T., Laan, P., Lancelot, C., Law, C. S., Levasseur, M., Marchetti, A., Millero, F. J., Nishioka, J., Nojiri, Y., Van Oijen, T., Riebesell, U., Rijkenberg, M. J. A., Saito, H., Takeda, S., Timmermans, K. R., Veldhuis, M. J. W., Waite, A. M., and Wong, C.: Synthesis of iron fertilization experiments: From the Iron Age in the Age of Enlightenment, J. Geophys. Res., 110, 2004JC002601, https://doi.org/10.1029/2004JC002601, 2005.

De Baar, H. J. W., Timmermans, K. R., Laan, P., De Porto, H. H., Ober, S., Blom, J. J., Bakker, M. C., Schilling, J., Sarthou, G., and Smit, M. G.: Titan: A new facility for ultraclean sampling of trace elements and isotopes in the deep oceans in the international Geotraces program, Mar. Chem., 111, 4–21, 2008.

De Cáceres, M. and Legendre, P.: Associations between species and groups of sites: indices and statistical inference, Ecology, 90, 12, https://doi.org/10.1890/08-1823.1, 2009.

De Lavergne, C., Palter, J. B., Galbraith, E. D., Bernardello, R., and Marinov, I.: Cessation of deep convection in the open Southern Ocean under anthropogenic climate change, Nat. Clim. Change, 4, 278–282, 2014.

Deppeler, S. L. and Davidson, A. T.: Southern Ocean phytoplankton in a changing climate, Front. Mar. Sci., 4, 40, https://doi.org/10.3389/fmars.2017.00040, 2017.

Drijfhout, S. S., Bull, C. Y. S., Hewitt, H., Holland, P. R., Jenkins, A., Mathiot, P., and Garabato, A. N.: An Amundsen Sea source of decadal temperature changes on the Antarctic continental shelf, Ocean Dynam., 74, 37–52, https://doi.org/10.1007/s10236-023-01587-3, 2024.

Eich, C., Pont, S. B., and Brussaard, C. P.: Effects of UV radiation on the chlorophyte *Micromonas polaris* host–virus interactions and MpoV-45*T* virus infectivity, Microorganisms, 9, 2429, https://doi.org/10.3390/microorganisms9122429, 2021.

Eich, C., Biggs, T. E., van de Poll, W. H., van Manen, M., Tian, H.-A., Jung, J., Lee, Y., Middag, R., and Brussaard, C. P.: Ecological importance of viral lysis as a loss factor of phytoplankton in the Amundsen Sea, Microorganisms, 10, 1967, https://doi.org/10.3390/microorganisms10101967, 2022.

Fahrbach, E., Hoppema, M., Rohardt, G., Schröder, M., and Wisotzki, A.: Decadal-scale variations of water mass properties in the deep Weddell Sea, Ocean Dynam., 54, 77–91, 2004.

Feng, Y., Hare, C. E., Rose, J. M., Handy, S. M., DiTullio, G. R., Lee, P. A., Smith Jr., W. O., Peloquin, J., Tozzi, S., Sun, J., Zhang, Y., Dunbar, R. B., Long, M. C., Sohst, B., Lohan, M., and Hutchins, D. A.: Interactive effects of iron, irradiance and CO_2 on Ross Sea phytoplankton, Deep-Sea Res. Pt. I, 57, 368–383, https://doi.org/10.1016/j.dsr.2009.10.013, 2010.

Fisher, B. J., Poulton, A. J., Meredith, M. P., Baldry, K., Schofield, O., and Henley, S. F.: Biogeochemistry of climate driven shifts in Southern Ocean primary producers, Biogeosciences Discuss. [preprint], https://doi.org/10.5194/bg-2023-10, 2023.

Fourquez, M., Janssen, D. J., Conway, T. M., Cabanes, D., Ellwood, M. J., Sieber, M., Trimborn, S., and Hassler, C.: Chasing iron bioavailability in the Southern Ocean: Insights from *Phaeocystis antarctica* and iron speciation, Sci. Adv., 9, eadf9696, https://doi.org/10.1126/sciadv.adf9696, 2023.

Friedlingstein, P., O'Sullivan, M., Jones, M. W., Andrew, R. M., Gregor, L., Hauck, J., Le Quéré, C., Luijkx, I. T., Olsen, A., Peters, G. P., Peters, W., Pongratz, J., Schwingshackl, C., Sitch, S., Canadell, J. G., Ciais, P., Jackson, R. B., Alin, S. R., Alkama, R., Arneth, A., Arora, V. K., Bates, N. R., Becker, M., Bellouin, N., Bittig, H. C., Bopp, L., Chevallier, F., Chini, L. P., Cronin, M., Evans, W., Falk, S., Feely, R. A., Gasser, T., Gehlen, M., Gkritzalis, T., Gloege, L., Grassi, G., Gruber, N., Gürses, Ö., Harris, I., Hefner, M., Houghton, R. A., Hurtt, G. C., Iida, Y., Ilyina, T., Jain, A. K., Jersild, A., Kadono, K., Kato, E., Kennedy, D., Klein Goldewijk, K., Knauer, J., Korsbakken, J. I., Landschützer, P., Lefèvre, N., Lindsay, K., Liu, J., Liu, Z., Marland, G., Mayot, N., McGrath, M. J., Metzl, N., Monacci, N. M., Munro, D. R., Nakaoka, S.-I., Niwa, Y., O'Brien, K., Ono, T., Palmer, P. I., Pan, N., Pierrot, D., Pocock, K., Poulter, B., Resplandy, L., Robertson, E., Rödenbeck, C., Rodriguez, C., Rosan, T. M., Schwinger, J., Séférian, R., Shutler, J. D., Skjelvan, I., Steinhoff, T., Sun, Q., Sutton, A. J., Sweeney, C., Takao, S., Tanhua, T., Tans, P. P., Tian, X., Tian, H., Tilbrook, B., Tsujino, H., Tubiello, F., van der Werf, G. R., Walker, A. P., Wanninkhof, R., Whitehead, C., Willstrand Wranne, A., Wright, R., Yuan, W., Yue, C., Yue, X., Zaehle, S., Zeng, J., and Zheng, B.: Global Carbon Budget 2022, Earth Syst. Sci. Data, 14, 4811–4900, https://doi.org/10.5194/essd-14-4811-2022, 2022.

Fukuda, R., Ogawa, H., Nagata, T., and Koike, I.: Direct Determination of Carbon and Nitrogen Contents of Natural Bacterial Assemblages in Marine Environments, Appl. Environ. Microbiol., 64, 3352–3358, https://doi.org/10.1128/AEM.64.9.3352-3358.1998, 1998.

Garrison, D. L., Gowing, M. M., Hughes, M. P., Campbell, L., Caron, D. A., Dennett, M. R., Shalapyonok, A., Olson, R. J., Landry, M. R., Brown, S. L., Liu, H.-B., Azam, F., Steward, G. F., Ducklow, H. W., and Smith, D. C.: Microbial food web structure in the Arabian Sea: a US JGOFS study, Deep-Sea Res. Pt. II, 47, 1387–1422, https://doi.org/10.1016/S0967-0645(99)00148-4, 2000.

Geider, R. J.: Light and temperature dependence of the carbon to chlorophyll a ratio in microalgae and cyanobacteria: implications for physiology and growth of phytoplankton, New Phytol., 106, 1–34, http://www.jstor.org/stable/2434683 (last access: 30 September 2024), 1987.

Geider, R. J. and La Roche, J.: The role of iron in phytoplankton photosynthesis, and the potential for iron-limitation of primary productivity in the sea, Photosynth. Res., 39, 275–301, 1994.

Gerringa, L. J., Alderkamp, A.-C., Laan, P., Thuroczy, C.-E., De Baar, H. J., Mills, M. M., van Dijken, G. L., van Haren, H., and Arrigo, K. R.: Iron from melting glaciers fuels the phytoplankton blooms in Amundsen Sea (Southern Ocean): Iron biogeochemistry, Deep-Sea Res. Pt. II, 71, 16–31, 2012.

Gerringa, L. J. A., Alderkamp, A.-C., Laan, P., Thuróczy, C.-E., De Baar, H. J. W., Mills, M. M., van Dijken, G. L., van Haren, H., and Arrigo, K. R.: Corrigendum to "Iron from melting glaciers fuels the phytoplankton blooms in Amundsen Sea (Southern Ocean): iron biogeochemistry" (Gerringa et al., 2012), Deep-Sea Res. Pt. II, 177, 104843, 2020.

Gledhill, M. and Buck, K. N.: The organic complexation of iron in the marine environment: a review, Front. Microbiol., 3, 69, https://doi.org/10.3389/fmicb.2012.00069, 2012.

Gómez-Valdivia, F., Holland, P. R., Siahaan, A., Dutrieux, P., and Young, E.: Projected West Antarctic Ocean Warming Caused by an Expansion of the Ross Gyre, Geophys. Res. Lett., 50, e2023GL102978, https://doi.org/10.1029/2023GL102978, 2023.

Gordon, L. I., Jennings Jr, J. C., Ross, A. A., and Krest, J. M.: A suggested protocol for continuous flow automated analysis of seawater nutrients (phosphate, nitrate, nitrite and silicic acid) in the WOCE Hydrographic Program and the Joint Global Ocean Fluxes Study, WOCE hydrographic program office, Methods Manual WHPO, WOCE hydrographic program office, methods manual WHPO, 1–52, https://www2.whoi.edu/site/wp-content/uploads/sites/84/2019/07/gordnut_133885.pdf (last access: 23 October 2024), 1993.

Greene, R. M., Geider, R. J., Kolber, Z., and Falkowski, P. G.: Iron-Induced Changes in Light Harvesting and Photochemical Energy Conversion Processes in Eukaryotic Marine Algae 1, Plant Physiol., 100, 565–575, 1992.

Grise, K. M., Polvani, L. M., Tselioudis, G., Wu, Y., and Zelinka, M. D.: The ozone hole indirect effect: Cloud-radiative anomalies accompanying the poleward shift of the eddy-driven jet in the Southern Hemisphere, Geophys. Res. Lett., 40, 3688–3692, https://doi.org/10.1002/grl.50675, 2013.

Hassler, C. S. and Schoemann, V.: Bioavailability of organically bound Fe to model phytoplankton of the Southern Ocean, Biogeosciences, 6, 2281–2296, https://doi.org/10.5194/bg-6-2281-2009, 2009.

Hawco, N. J., Tagliabue, A., and Twining, B. S.: Manganese Limitation of Phytoplankton Physiology and Productivity in the Southern Ocean, Global Biogeochem. Cy., 36, e2022GB007382, https://doi.org/10.1029/2022GB007382, 2022.

Hillenbrand, C.-D. and Cortese, G.: Polar stratification: A critical view from the Southern Ocean, Palaeogeogr. Palaeocl., 242, 240–252, 2006.

Hinz, D. J., Nielsdóttir, M. C., Korb, R. E., Whitehouse, M. J., Poulton, A. J., Moore, C. M., Achterberg, E. P., and Bibby, T. S.: Responses of microplankton community structure to iron addition in the Scotia Sea, Deep-Sea Res. Pt. II, 59/60, 36–46, https://doi.org/10.1016/j.dsr2.2011.08.006, 2012.

Hoppema, M., Middag, R., de Baar, H. J., Fahrbach, E., van Weerlee, E. M., and Thomas, H.: Whole season net community production in the Weddell Sea, Polar Biol., 31, 101–111, 2007.

Hopwood, M. J., Carroll, D., Höfer, J., Achterberg, E. P., Meire, L., Le Moigne, F. A., Bach, L. T., Eich, C., Sutherland, D. A., and González, H. E.: Highly variable iron content modulates iceberg-ocean fertilisation and potential carbon export, Nat. Commun., 10, 5261, https://doi.org/10.1038/s41467-019-13231-0, 2019.

Huang, Y., Fassbender, A. J., and Bushinsky, S. M.: Biogenic carbon pool production maintains the Southern Ocean carbon sink, P. Natl. Acad. Sci. USA, 120, e2217909120, https://doi.org/10.1073/pnas.2217909120, 2023.

Hutchins, D. A. and Boyd, P. W.: Marine phytoplankton and the changing ocean iron cycle, Nat. Clim. Change, 6, 1072–1079, 2016.

Hutchins, D. A. and Bruland, K. W.: Iron-limited diatom growth and Si : N uptake ratios in a coastal upwelling regime, Nature, 393, 561–564, https://doi.org/10.1038/31203, 1998.

Jabre, L. and Bertrand, E. M.: Interactive effects of iron and temperature on the growth of *Fragilariopsis cylindrus* , Limnol. Oceanogr. Lett., 5, 363–370, 2020.

Jabre, L. J., Allen, A. E., McCain, J. S. P., McCrow, J. P., Tenenbaum, N., Spackeen, J. L., Sipler, R. E., Green, B. R., Bronk, D. A., Hutchins, D. A., and Bertrand, E. M.: Molecular underpinnings and biogeochemical consequences of enhanced diatom growth in a warming Southern Ocean, P. Natl. Acad. Sci. USA, 118, e2107238118, https://doi.org/10.1073/pnas.2107238118, 2021.

Jensen, L. T., Wyatt, N. J., Landing, W. M., and Fitzsimmons, J. N.: Assessment of the stability, sorption, and exchangeability of marine dissolved and colloidal metals, Mar. Chem., 220, 103754, https://doi.org/10.1016/j.marchem.2020.103754, 2020.

Jeon, M. H., Jung, J., Park, M. O., Aoki, S., Kim, T. W., and Kim, S. K.: Tracing Circumpolar Deep Water and glacial meltwater using humic-like fluorescent dissolved organic matter in the Amundsen Sea, Antarctica, 235, 104008, 2021.

Karakuş, O., Völker, C., Iversen, M., Hagen, W., and Hauck, J.: The Role of Zooplankton Grazing and Nutrient Recycling for Global Ocean Biogeochemistry and Phytoplankton Phenology, J. Geophys. Res.-Biogeo., 127, e2022JG006798, https://doi.org/10.1029/2022JG006798, 2022.

Kelleher, M. K. and Grise, K. M.: Varied midlatitude shortwave cloud radiative responses to Southern Hemisphere circulation shifts, Atmos. Sci. Lett., 23, e1068, https://doi.org/10.1002/asl.1068, 2022.

Klunder, M. B., Laan, P., Middag, R., De Baar, H. J. W., and Van Ooijen, J. C.: Dissolved iron in the Southern Ocean (Atlantic sector), Deep-Sea Res. Pt. II, 58, 2678–2694, 2011.

Klunder, M. B., Laan, P., De Baar, H. J. W., Middag, R., Neven, I., and Van Ooijen, J.: Dissolved Fe across the Weddell Sea and Drake Passage: impact of DFe on nutrient uptake, Biogeosciences, 11, 651–669, https://doi.org/10.5194/bg-11-651-2014, 2014.

Kranzler, C. F., Brzezinski, M. A., Cohen, N. R., Lampe, R. H., Maniscalco, M., Till, C. P., Mack, J., Latham, J. R., Bruland, K. W., and Twining, B. S.: Impaired viral infection and reduced mortality of diatoms in iron-limited oceanic regions, Nat. Geosci., 14, 231–237, 2021.

Kroh, G. E. and Pilon, M.: Regulation of iron homeostasis and use in chloroplasts, Int. J. Molecul. Sci., 21, 3395, https://doi.org/10.3390/ijms21093395, 2020.

Krumhardt, K. M., Long, M. C., Sylvester, Z. T., and Petrik, C. M.: Climate drivers of Southern Ocean phytoplankton community composition and potential impacts on higher trophic levels, Front. Mar. Sci., 9, 916140, https://doi.org/10.3389/fmars.2022.916140, 2022.

Kustka, A. B., Allen, A. E., and Morel, F. M.: Sequence analysis and transcriptional regulation of iron acquisition genes in two marine diatoms 1, J. Phycol., 43, 715–729, 2007.

Lampe, R. H., Mann, E. L., Cohen, N. R., Till, C. P., Thamatrakoln, K., Brzezinski, M. A., Bruland, K. W., Twining, B. S., and Marchetti, A.: Different iron storage strategies among bloom-forming diatoms, P. Natl. Acad. Sci. USA, 115, E12275–E12284, https://doi.org/10.1073/pnas.1805243115, 2018.

Lane, E. S., Jang, K., Cullen, J. T., and Maldonado, M. T.: The interaction between inorganic iron and cadmium uptake in the marine diatom Thalassiosira oceanica, Limnol. Oceanogr., 53, 1784–1789, 2008.

Lannuzel, D., Vancoppenolle, M., van Der Merwe, P., De Jong, J., Meiners, K. M., Grotti, M., Nishioka, J., and Schoemann, V.: Iron in sea ice: Review and new insights, Elementa, 4, 000130, https://doi.org/10.12952/journal.elementa.000130, 2016.

Latour, P., Strzepek, R. F., Wuttig, K., van der Merwe, P., Bach, L. T., Eggins, S., Boyd, P. W., Ellwood, M. J., Pinfold, T. L., and Bowie, A. R.: Seasonality of phytoplankton growth limitation by iron and manganese in subantarctic waters, Elementa, 11, 1, https://doi.org/10.1525/elementa.2023.00022, 2023.

Latour, P., Eggins, S., Van Der Merwe, P., Bach, L. T., Boyd, P. W., Ellwood, M. J., Bowie, A. R., Wuttig, K., and Strzepek, R. F.: Characterization of a Southern Ocean deep chlorophyll maximum: Response of phytoplankton to light, iron, and manganese enrichment, Limnol. Oceanogr. Lett., 9, 145–154, https://doi.org/10.1002/lol2.10366, 2024.

Laufkötter, C., Vogt, M., Gruber, N., Aita-Noguchi, M., Aumont, O., Bopp, L., Buitenhuis, E., Doney, S. C., Dunne, J., Hashioka, T., Hauck, J., Hirata, T., John, J., Le Quéré, C., Lima, I. D., Nakano, H., Seferian, R., Totterdell, I., Vichi, M., and Völker, C.: Drivers and uncertainties of future global marine primary production in marine ecosystem models, Biogeosciences, 12, 6955–6984, https://doi.org/10.5194/bg-12-6955-2015, 2015.

Laws, E. A. and Bannister, T. T.: Nutrient-and light-limited growth of Thalassiosira fluviatilis in continuous culture, with implications for phytoplankton growth in the ocean 1, Limnol. Oceanogr., 25, 457–473, 1980.

Lenth, R.: _emmeans: Estimated Marginal Means, aka Least-Squares Means_, version 1.10.0, https://CRAN.R-project.org/package=emmeans (last access: 23 October 2024), 2016.

Leung, S., Cabré, A., and Marinov, I.: A latitudinally banded phytoplankton response to 21st century climate change in the Southern Ocean across the CMIP5 model suite, Biogeosciences, 12, 5715–5734, https://doi.org/10.5194/bg-12-5715-2015, 2015.

Lewandowska, A. and Sommer, U.: Climate change and the spring bloom: a mesocosm study on the influence of light and temperature on phytoplankton and mesozooplankton, Mar. Ecol. Prog. Ser., 405, 101–111, 2010.

Maat, D. S., Biggs, T., Evans, C., Van Bleijswijk, J. D. L., Van der Wel, N. N., Dutilh, B. E., and Brussaard, C. P. D.: Characterization and Temperature Dependence of Arctic *Micromonas polaris* Viruses, Viruses, 9, 134, https://doi.org/10.3390/v9060134, 2017.

Mackey, M. D., Mackey, D. J., Higgins, H. W., and Wright, S. W.: CHEMTAX-a program for estimating class abundances from chemical markers: application to HPLC measurements of phytoplankton, Mar. Ecol. Prog. Ser., 144, 265–283, 1996.

Mangiafico, S. S.: rcompanion: Functions to Support Extension Education Program Evaluation, version 2.4.34, Rutgers Cooperative Extension, https://CRAN.R-project.org/package=rcompanion (last access: 23 October 2024), 2023.

Marie, D., Partensky, F., Vaulot, D., and Brussaard, C.: Enumeration of Phytoplankton, Bacteria, and Viruses in Marine Samples, CP Cytometry, 10, 18770685, https://doi.org/10.1002/0471142956.cy1111s10, 1999.

Martin, J. H., Fitzwater, S. E., and Gordon, R. M.: Iron deficiency limits phytoplankton growth in Antarctic waters, Global Biogeochem. Cy., 4, 5–12, 1990.

McCain, J. S. P., Tagliabue, A., Susko, E., Achterberg, E. P., Allen, A. E., and Bertrand, E. M.: Cellular costs underpin micronutrient limitation in phytoplankton, Sci. Adv., 7, eabg6501, https://doi.org/10.1126/sciadv.abg6501, 2021.

Meredith, M., Sommerkorn, M., Cassotta, S., Derksen, C., Ekaykin, A., Hollowed, A., Kofinas, G., Mackintosh, A., Melbourne-Thomas, J., Muelbert, M. M. C., Ottersen, G., Pritchard, H., and Schuur, E. A. G.: Chap. 3, IPCC Polar regions — Special Report on the Ocean and Cryosphere in a Changing Climate, https://doi.org/10.1017/9781009157964, 2019.

Meyerink, S. W., Ellwood, M. J., Maher, W. A., Dean Price, G., and Strzepek, R. F.: Effects of iron limitation on silicon uptake kinetics and elemental stoichiometry in two Southern Ocean diatoms, *Eucampia antarctica* and *Proboscia inermis* , and the temperate diatom *Thalassiosira pseudonana*, Limnol. Oceanogr., 62, 2445–2462, https://doi.org/10.1002/lno.10578, 2017.

Middag, R., De Baar, H. J., Bruland, K. W., and Van Heuven, S. M.: The distribution of nickel in the West-Atlantic Ocean, its relationship with phosphate and a comparison to cadmium and zinc, Front. Mar. Sci., 7, 105, https://doi.org/10.3389/fmars.2020.00105, 2020.

Middag, R., Zitoun, R., and Conway, T.: Trace Metals, in: Marine Analytical Chemistry, edited by: Blasco, J. and Tovar-Sánchez, A., Springer International Publishing, Cham, 103–198, https://doi.org/10.1007/978-3-031-14486-8_3, 2023.

Millero, F. J., Sotolongo, S., and Izaguirre, M.: The oxidation kinetics of Fe (II) in seawater, Geochim. Cosmochim. Ac., 51, 793–801, 1987.

Milligan, A. J. and Harrison, P. J.: Effects of non-steady-state iron limitation on nitrogen assimilatory enzymes in the marine diatom *thalassiosira weissflogii* (BACILLARIOPHYCEAE), J. Phycol., 36, 78–86, https://doi.org/10.1046/j.1529-8817.2000.99013.x, 2000.

Mills, M. M., Alderkamp, A.-C., Thuróczy, C.-E., van Dijken, G. L., Laan, P., de Baar, H. J., and Arrigo, K. R.: Phytoplankton biomass and pigment responses to Fe amendments in the Pine Island and Amundsen polynyas, Deep-Sea Res. Pt. II, 71, 61–76, 2012.

Minas, H. J. and Minas, M.: Net community production in High nutrient-low chlorophyll waters of the tropical and Antarctic oceans-grazing vs. iron hypothesis, Oceanol. Acta, 15, 145–162, 1992.

Misumi, K., Lindsay, K., Moore, J. K., Doney, S. C., Bryan, F. O., Tsumune, D., and Yoshida, Y.: The iron budget in ocean surface waters in the 20th and 21st centuries: projections by the Community Earth System Model version 1, Biogeosciences, 11, 33–55, https://doi.org/10.5194/bg-11-33-2014, 2014.

Moore, C. M., Seeyave, S., Hickman, A. E., Allen, J. T., Lucas, M. I., Planquette, H., Pollard, R. T., and Poulton, A. J.: Iron-light interactions during the CROZet natural iron bloom and EXport experiment (CROZEX) I: Phytoplankton growth and photophysiology, Deep-Sea Res. Pt. II, 54, 2045–2065, https://doi.org/10.1016/j.dsr2.2007.06.011, 2007.

Moore, J. K., Fu, W., Primeau, F., Britten, G. L., Lindsay, K., Long, M., Doney, S. C., Mahowald, N., Hoffman, F., and Randerson, J. T.: Sustained climate warming drives declining marine biological productivity, Science, 359, 1139–1143, https://doi.org/10.1126/science.aao6379, 2018.

Morán, X. A. G., Sebastián, M., Pedrís-Alií, C., and Estrada, M.: Response of Southern Ocean phytoplankton and bacterioplankton production to short-term experimental warming, Limnol. Oceanogr., 51, 1791–1800, https://doi.org/10.4319/lo.2006.51.4.1791, 2006.

Moreau, S., Hattermann, T., de Steur, L., Kauko, H. M., Ahonen, H., Ardelan, M., Assmy, P., Chierici, M., Descamps, S., Dinter, T., Falkenhaug, T., Fransson, A., Grønningsæter, E., Hallfredsson, E. H., Huhn, O., Lebrun, A., Lowther, A., Lübcker, N., Monteiro, P., Peeken, I., Roychoudhury, A., Różańska, M., Ryan-Keogh, T., Sanchez, N., Singh, A., Simonsen, J. H., Steiger, N., Thomalla, S. J., van Tonder, A., Wiktor, J. M., and Steen, H.: Wind-driven upwelling of iron sustains dense blooms and food webs in the eastern Weddell Gyre, Nat. Commun., 14, 1303, https://doi.org/10.1038/s41467-023-36992-1, 2023.

Noiri, Y., Kudo, I., Kiyosawa, H., Nishioka, J., and Tsuda, A.: Influence of iron and temperature on growth, nutrient utilization ratios and phytoplankton species composition in the western subarctic Pacific Ocean during the SEEDS experiment, Prog. Oceanogr., 64, 149–166, 2005.

Ohnemus, D. C., Auro, M. E., Sherrell, R. M., Lagerström, M., Morton, P. L., Twining, B. S., Rauschenberg, S., and Lam, P. J.: Laboratory intercomparison of marine particulate digestions including Piranha: a novel chemical method for dissolution of polyethersulfone filters, Limnol. Ocean Method., 12, 530–547, https://doi.org/10.4319/lom.2014.12.530, 2014.

Oksanen, J., Simpson, G., Blanchet, F., Kindt, R., Legendre, P., Minchin, P., O'Hara, R., Solymos, P., Stevens, M., Szoecs, E., Wagner, H., Barbour, M., Bedward, M., Bolker, B., Borcard, D., Carvalho, G., Chirico, M., De Caceres, M., Durand, S.,Evangelista, H., FitzJohn, R., Friendly, M., Furneaux, B., Hannigan, G., Hill, M., Lahti, L., McGlinn, D., Ouellette, M., Ribeiro Cunha, E., Smith, T., Stier, A., Ter Braak, C., and Weedon, J.: vegan: Community Ecology Package, https://CRAN.R-project.org/package=vegan (last access: 23 October 2024), 2022.

Olson, R. J., Sosik, H. M., Chekalyuk, A. M., and Shalapyonok, A.: Effects of iron enrichment on phytoplankton in the Southern Ocean during late summer: Active fluorescence and flow cystometric analyses, Deep-Sea Res. Pt. II, 47, 3181–3200, https://doi.org/10.1016/S0967-0645(00)00064-3, 2000.

Park, J., Kuzminov, F. I., Bailleul, B., Yang, E. J., Lee, S., Falkowski, P. G., and Gorbunov, M. Y.: Light availability rather than Fe controls the magnitude of massive phytoplankton bloom in the Amundsen Sea polynyas, Antarctica, Limnol. Oceanogr., 62, 2260–2276, https://doi.org/10.1002/lno.10565, 2017.

Pausch, F., Bischof, K., and Trimborn, S.: Iron and manganese co-limit growth of the Southern Ocean diatom Chaetoceros debilis, PLOS ONE, 14, e0221959, https://doi.org/10.1371/journal.pone.0221959, 2019.

Peers, G. and Price, N. M.: A role for manganese in superoxide dismutases and growth of iron-deficient diatoms, Limnol. Oceanogr., 49, 1774–1783, https://doi.org/10.4319/lo.2004.49.5.1774, 2004.

Petrou, K., Kranz, S. A., Trimborn, S., Hassler, C. S., Ameijeiras, S. B., Sackett, O., Ralph, P. J., and Davidson, A. T.: Southern Ocean phytoplankton physiology in a changing climate, J. Plant Physiol., 203, 135–150, 2016.

Pinkerton, M. H., Boyd, P. W., Deppeler, S., Hayward, A., Höfer, J., and Moreau, S.: Evidence for the impact of climate change on primary producers in the Southern Ocean, Front. Ecol. Evol., 9, 592027, 2021.

Planquette, H. and Sherrell, R. M.: Sampling for particulate trace element determination using water sampling bottles: methodology and comparison to in situ pumps, Limnol. Oceanogr.-Method., 10, 367–388, 2012.

Primeau, F. W., Holzer, M., and DeVries, T.: Southern Ocean nutrient trapping and the efficiency of the biological pump, J. Geophys. Res.-Ocean., 118, 2547–2564, https://doi.org/10.1002/jgrc.20181, 2013.

Raiswell, R., Benning, L. G., Tranter, M., and Tulaczyk, S.: Bioavailable iron in the Southern Ocean: the significance of the iceberg conveyor belt, Geochem. Trans., 9, 7, https://doi.org/10.1186/1467-4866-9-7, 2008.

Raiswell, R., Hawkings, J. R., Benning, L. G., Baker, A. R., Death, R., Albani, S., Mahowald, N., Krom, M. D., Poulton, S. W., Wadham, J., and Tranter, M.: Potentially bioavailable iron delivery by iceberg-hosted sediments and atmospheric dust to the polar oceans, Biogeosciences, 13, 3887–3900, https://doi.org/10.5194/bg-13-3887-2016, 2016.

Raven, J. A.: Predictions of Mn and Fe use efficiencies of phototrophic growth as a function of light availability for growth and of C assimilation pathway, New Phytol., 116, 1–18, https://doi.org/10.1111/j.1469-8137.1990.tb00505.x, 1990.

R Core Team: R: A language and environment for statistical computing. R Foundation for Statistical Computing, Vienna, Austria, https://www.R-project.org/ (last access: 23 October 2024), 2021.

Reay, D. S., Priddle, J., Nedwell, D. B., Whitehouse, M. J., Ellis-Evans, J. C., Deubert, C., and Connelly, D. P.: Regulation by low temperature of phytoplankton growth and nutrient uptake in the Southern Ocean, Mar. Ecol. Prog. Ser., 219, 51–64, 2001.

Rignot, E., Jacobs, S., Mouginot, J., and Scheuchl, B.: Ice-Shelf Melting Around Antarctica, Science, 341, 266–270, https://doi.org/10.1126/science.1235798, 2013.

Rijkenberg, M. J., de Baar, H. J., Bakker, K., Gerringa, L. J., Keijzer, E., Laan, M., Laan, P., Middag, R., Ober, S., and van Ooijen, J.: "PRISTINE", a new high volume sampler for ultraclean sampling of trace metals and isotopes, Mar. Chem., 177, 501–509, 2015.

Rose, J. M., Feng, Y., DiTullio, G. R., Dunbar, R. B., Hare, C. E., Lee, P. A., Lohan, M., Long, M., W. O. Smith Jr., Sohst, B., Tozzi, S., Zhang, Y., and Hutchins, D. A.: Synergistic effects of iron and temperature on Antarctic phytoplankton and microzooplankton assemblages, Biogeosciences, 6, 3131–3147, https://doi.org/10.5194/bg-6-3131-2009, 2009.

Ryan-Keogh, T. J., Thomalla, S. J., Monteiro, P. M., and Tagliabue, A.: Multidecadal trend of increasing iron stress in Southern Ocean phytoplankton, Science, 379, 834–840, 2023.

Ryderheim, F., Grønning, J., and Kiørboe, T.: Thicker shells reduce copepod grazing on diatoms, Limnol. Oceanogr. Lett., 7, 435–442, 2022.

Sallée, J. B., Pellichero, V., Akhoudas, C.,Pauthenet, E., Vignes, L., Schmidtko, S., Garabato, A. N., Sutherland, P., and Kuusela, M.: Summertime increases in upper-ocean stratification and mixed-layer depth, Nature, 591, 592–598, 2021.

Sarmiento, J. L., Gruber, N., Brzezinski, M. A., and Dunne, J. P.: High-latitude controls of thermocline nutrients and low latitude biological productivity, Nature, 427, 56–60, https://doi.org/10.1038/nature02127, 2004.

Scharek, R., Van Leeuwe, M. A., and De Baar, H. J. W.: Responses of Southern Ocean phytoplankton to the addition of trace metals, Deep-Sea Res. Pt. II, 44, 209–227, 1997.

Schoffman, H., Lis, H., Shaked, Y., and Keren, N.: Iron–Nutrient Interactions within Phytoplankton, Front. Plant Sci., 7, 1223, https://doi.org/10.3389/fpls.2016.01223, 2016.

Schofield, O., Miles, T., Alderkamp, A.-C., Lee, S., Haskins, C., Rogalsky, E., Sipler, R., Sherrell, R. M., and Yager, P. L.: In situ phytoplankton distributions in the Amundsen Sea Polynya measured by autonomous gliders, Elementa, 3, 000073, https://doi.org/10.12952/journal.elementa.000073, 2015.

Selz, V., Lowry, K. E., Lewis, K. M., Joy-Warren, H. L., van de Poll, W., Nirmel, S., Tong, A., and Arrigo, K. R.: Distribution of Phaeocystis antarctica-dominated sea ice algal communities and their potential to seed phytoplankton across the western Antarctic Peninsula in spring, Mar. Ecol. Prog. Ser., 586, 91–112, 2018.

Seyitmuhammedov, K., Stirling, C. H., Reid, M. R., van Hale, R., Laan, P., Arrigo, K. R., van Dijken, G., Alderkamp, A.-C., and Middag, R.: The distribution of Fe across the shelf of the Western Antarctic Peninsula at the start of the phytoplankton growing season, Mar. Chem., 238, 104066, https://doi.org/10.1016/j.marchem.2021.104066, 2022.

Shaw, T. J., Smith Jr, K. L., Hexel, C. R., Dudgeon, R., Sherman, A. D., Vernet, M., and Kaufmann, R. S.: 234Th-based carbon export around free-drifting icebergs in the Southern Ocean, Deep-Sea Res. Pt. II, 58, 1384–1391, 2011.

Sherrell, R. M., Lagerström, M. E., Forsch, K. O., Stammerjohn, S. E., and Yager, P. L.: Dynamics of dissolved iron and other bioactive trace metals (Mn, Ni, Cu, Zn) in the Amundsen Sea Polynya, Antarctica, Elementa, 3, 000071, https://doi.org/10.12952/journal.elementa.000071, 2015.

Shi, J.-R., Talley, L. D., Xie, S.-P., Liu, W., and Gille, S. T.: Effects of buoyancy and wind forcing on Southern Ocean climate change, J. Clim., 33, 10003–10020, 2020.

Sieber, M., Conway, T. M., de Souza, G. F., Hassler, C. S., Ellwood, M. J., and Vance, D.: Isotopic fingerprinting of biogeochemical processes and iron sources in the iron-limited surface Southern Ocean, Earth Planet. Sc. Lett., 567, 116967, https://doi.org/10.1016/j.epsl.2021.116967, 2021.

Sinha, A. K., Parli Venkateswaran, B., Tripathy, S. C., Sarkar, A., and Prabhakaran, S.: Effects of growth conditions on siderophore producing bacteria and siderophore production from Indian Ocean sector of Southern Ocean, J. Basic Microbiol., 59, 412–424, https://doi.org/10.1002/jobm.201800537, 2019.

Slagter, H. A., Gerringa, L. J. A., and Brussaard, C. P. D.: Phytoplankton Virus Production Negatively Affected by Iron Limitation, Front. Mar. Sci., 3, 156, https://doi.org/10.3389/fmars.2016.00156, 2016.

Stapleford, L. S. and Smith, R. E.: The interactive effects of temperature and silicon limitation on the psychrophilic ice diatom Pseudonitszchia seriata, Polar Biol., 16, 589–594, 1996.

Strass, V. H., Rohardt, G., Kanzow, T., Hoppema, M., and Boebel, O.: Multidecadal Warming and Density Loss in the Deep Weddell Sea, Antarctica, J. Clim., 33, 9863–9881, https://doi.org/10.1175/JCLI-D-20-0271.1, 2020.

Strzepek, R. F., Boyd, P. W., and Sunda, W. G.: Photosynthetic adaptation to low iron, light, and temperature in Southern Ocean phytoplankton, P. Natl. Acad. Sci. USA, 116, 4388–4393, 2019.

Tagliabue, A., Aumont, O., DeAth, R., Dunne, J. P., Dutkiewicz, S., Galbraith, E., Misumi, K., Moore, J. K., Ridgwell, A., Sherman, E., Stock, C., Vichi, M., Völker, C., and Yool, A.: How well do global ocean biogeochemistry models simulate dissolved iron distributions?, Global Biogeochem. Cy., 30, 149–174, https://doi.org/10.1002/2015GB005289, 2016.

Takahashi, T., Sweeney, C., Hales, B., Chipman, D. W., Newberger, T., Goddard, J. G., Iannuzzi, R. A., and Sutherland, S. C.: The changing carbon cycle in the Southern Ocean, Oceanography, 25, 26–37, 2012.

Taylor, S. R. and McLennan, S. M.: The continental crust: its composition and evolution, Blackwell Scientific Publications (Oxford), 312 pp., ISBN 0-632-01148-3, 1985.

Teske, V., Timmermann, R., and Semmler, T.: Subsurface warming in the Antarctica's Weddell Sea can be avoided by reaching the 2 °C warming target, Commun. Earth Environ., 5, 93, https://doi.org/10.1038/s43247-024-01238-5, 2024.

Thomalla, S. J., Nicholson, S.-A., Ryan-Keogh, T. J., and Smith, M. E.: Widespread changes in Southern Ocean phytoplankton blooms linked to climate drivers, Nat. Clim. Change, 13, 975–984, 2023.

Tian, H. A.: Sources and biogeochemistry of bio-active trace metals in the Southern Ocean and coastal Antarctica: perspectives from their isotopes, PhD thesis, Utrecht Studies In Earth Sciences, Utrecht University, the Netherlands, 286 pp., https://doi.org/10.33540/2106, 2024.

Turner, J., Colwell, S. R., Marshall, G. J., Lachlan-Cope, T. A., Carleton, A. M., Jones, P. D., Lagun, V., Reid, P. A., and Iagovkina, S.: Antarctic climate change during the last 50 years, Int. J. Climatol., 25, 279–294, 2005.

Twining, B. S. and Baines, S. B.: The trace metal composition of marine phytoplankton, Annu. Rev. Mar. Sci., 5, 191–215, 2013.

Twining, B. S., Baines, S. B., and Fisher, N. S.: Element stoichiometries of individual plankton cells collected during the Southern Ocean Iron Experiment (SOFeX), Limnol. Oceanogr., 49, 2115–2128, 2004.

van der Merwe, P., Wuttig, K., Holmes, T., Trull, T. W., Chase, Z., Townsend, A. T., Goemann, K., and Bowie, A. R.: High lability Fe particles sourced from glacial erosion can meet previously unaccounted biological demand: Heard Island, Southern Ocean, Front. Mar. Sci., 6, 332, https://doi.org/10.3389/fmars.2019.00332, 2019.

Van Heukelem, L. and Thomas, C. S.: Computer-assisted high-performance liquid chromatography method development with applications to the isolation and analysis of phytoplankton pigments, J. Chromatogr. A, 910, 31–49, 2001.

van Haren, H., Brussaard, C. P. D., Gerringa, L. J. A., van Manen, M. H., Middag, R., and Groenewegen, R.: Diapycnal mixing across the photic zone of the NE Atlantic, Ocean Sci., 17, 301–318, https://doi.org/10.5194/os-17-301-2021, 2021.

Van Leeuwe, M. A., Villerius, L. A., Roggeveld, J., Visser, R. J. W., and Stefels, J.: An optimized method for automated analysis of algal pigments by HPLC, Mar. Chem., 102, 267–275, 2006.

Van Manen, M., Aoki, S., Brussaard, C. P., Conway, T. M., Eich, C., Gerringa, L. J., Jung, J., Kim, T.-W., Lee, S., and Lee, Y.: The role of the Dotson Ice Shelf and Circumpolar Deep Water as driver and source of dissolved and particulate iron and manganese in the Amundsen Sea polynya, Southern Ocean, Mar. Chem., 246, 104161, https://doi.org/10.1016/j.marchem.2022.104161, 2022.

van Oijen, T., Van Leeuwe, M. A., Granum, E., Weissing, F. J., Bellerby, R. G. J., Gieskes, W. W. C., and De Baar, H. J. W.: Light rather than iron controls photosynthate production and allocation in Southern Ocean phytoplankton populations during austral autumn, J. Plank. Res., 26, 885–900, 2004.

Veldhuis, M. J. and Kraay, G. W.: Phytoplankton in the subtropical Atlantic Ocean: towards a better assessment of biomass and composition, Deep-Sea Res. Pt. I, 51, 507–530, 2004.

Venables, H. and Moore, C. M.: Phytoplankton and light limitation in the Southern Ocean: Learning from high-nutrient, high-chlorophyll areas, J. Geophys. Res.-Ocean., 115, C02015, https://doi.org/10.1029/2009JC005361, 2010.

Verardo, D. J., Froelich, P. N., and McIntyre, A.: Determination of organic carbon and nitrogen in marine sediments using the Carlo Erba NA-1500 Analyzer, Deep-Sea Res. Pt. A, 37, 157–165, 1990.

Viljoen, J. J., Philibert, R., Van Horsten, N., Mtshali, T., Roychoudhury, A. N., Thomalla, S., and Fietz, S.: Phytoplankton response in growth, photophysiology and community structure to iron and light in the Polar Frontal Zone and Antarctic waters, Deep-Sea Res. Pt. I, 141, 118–129, https://doi.org/10.1016/j.dsr.2018.09.006, 2018.

Vives, C. R., Schallenberg, C., Strutton, P. G., and Westwood, K. J.: Iron and light limitation of phytoplankton growth off East Antarctica, J. Mar. Syst., 234, 103774, https://doi.org/10.1016/j.jmarsys.2022.103774, 2022.

von Berg, L., Prend, C. J., Campbell, E. C., Mazloff, M. R., Talley, L. D., and Gille, S. T.: Weddell Sea Phytoplankton Blooms Modulated by Sea Ice Variability and Polynya Formation, Geophys. Res. Lett., 47, e2020GL087954, https://doi.org/10.1029/2020GL087954, 2020.

Voronina, N. M., Kosobokova, K. N., and Pakhomov, E. A.: Composition and biomass of summer metazoan plankton in the 0–200 m

layer of the Atlantic sector of the Antarctic, Polar Biol., 14, 91–95, https://doi.org/10.1007/BF00234970, 1994.

Waite, A. M. and Nodder, S. D.: The effect of in situ iron addition on the sinking rates and export flux of Southern Ocean diatoms, Deep-Sea Res. Pt. II., 48, 2635–2654, 2001.

Wang, X. J., Behrenfeld, M., Le Borgne, R., Murtugudde, R., and Boss, E.: Regulation of phytoplankton carbon to chlorophyll ratio by light, nutrients and temperature in the Equatorial Pacific Ocean: a basin-scale model, Biogeosciences, 6, 391–404, https://doi.org/10.5194/bg-6-391-2009, 2009.

Wickham, H.: ggplot2: Elegant Graphics for Data Analysis, Springer-Verlag, New York, ISBN 978-3-319-24277-4, 2016.

Wolfe-Simon, F., Grzebyk, D., Schofield, O., and Falkowski, P. G.: The role and evolution of superoxide dismutases in algae, J. Phycol., 41, 453–465, https://doi.org/10.1111/j.1529-8817.2005.00086.x, 2005.

Worden, A. Z., Nolan, J. K., and Palenik, B.: Assessing the dynamics and ecology of marine picophytoplankton: The importance of the eukaryotic component, Limnol. Oceanogr., 49, 168–179, https://doi.org/10.4319/lo.2004.49.1.0168, 2004.

Wu, M., McCain, J. S. P., Rowland, E., Middag, R., Sandgren, M., Allen, A. E., and Bertrand, E. M.: Manganese and iron deficiency in Southern Ocean *Phaeocystis antarctica* populations revealed through taxon-specific protein indicators, Nat. Commun., 10, 3582, https://doi.org/10.1038/s41467-019-11426-z, 2019.

Yoon, J.-E., Yoo, K.-C., Macdonald, A. M., Yoon, H.-I., Park, K.-T., Yang, E. J., Kim, H.-C., Lee, J. I., Lee, M. K., Jung, J., Park, J., Lee, J., Kim, S., Kim, S.-S., Kim, K., and Kim, I.-N.: Reviews and syntheses: Ocean iron fertilization experiments – past, present, and future looking to a future Korean Iron Fertilization Experiment in the Southern Ocean (KIFES) project, Biogeosciences, 15, 5847–5889, https://doi.org/10.5194/bg-15-5847-2018, 2018.

Zhu, Z., Xu, K., Fu, F., Spackeen, J. L., Bronk, D. A., and Hutchins, D. A.: A comparative study of iron and temperature interactive effects on diatoms and *Phaeocystis antarctica* from the Ross Sea, Antarctica, Mar. Ecol. Prog. Ser., 550, 39–51, 2016.